

Politecnico di Torino Master's Degree in Aerospace Engineering

Master Thesis

PRELIMINARY DESIGN OF LOCOMOTION SYSTEM FOR A LUNAR PRESSURIZED ROVER

Supervisor:

Candidate:

Prof. Alfonso Pagani, DIMEAS

Ludovica Giacconi, 315886

Co-supervisors:

Prof. Erasmo Carrera, DIMEAS

Prof. Marco Petrolo, DIMEAS

Prof. Giuseppe Palaia, DIMEAS

Prof. Karim Abu Salem, DIMEAS

Contents

A	bstra	ct	1
C	ontex	at of the Work	2
1	Intr	roduction	3
2	Ger	neral Context	4
	2.1	Lunar environment	4
		2.1.1 Temperatures	4
		2.1.2 Meteoroid bombardment	4
		2.1.3 Ionizing radiation	5
		2.1.4 Dust	5
	2.2	Surface exploration vehicles - State of art	6
		2.2.1 Unpressurized rovers	7
		2.2.2 Pressurized rovers	8
	2.3	Pressurized rover configurations - State of art	10
		2.3.1 Single cylinder configuration	10
		2.3.2 Multi-segmented configuration	10
		2.3.3 Dual cylinder configuration	11
	2.4	Mobility Systems - State of art	11
3	Mis	sion and Requirements	22
	3.1	Mission Overview	22
	3.2	Requirements	22
	3.3	Reference Traverse	27
4	Pre	ssurized Rover Preliminary Design	30
	4.1	Geometrical configurations	30
		4.1.1 Configuration trade-off	31
		4.1.2 Configuration chosen	32
		4.1.3 Fairing integration	32
	4.2	Preliminary Design and Sizing	33
		4.2.1 Overall dimensions	33

	4.3	Subsystems	9
		4.3.1 Structure	9
		4.3.2 Mobility	0
		4.3.3 TCS	0
		4.3.4 EPS	0
		4.3.5 GNC	0
		4.3.6 ECLSS	0
		4.3.7 CDH	1
		4.3.8 COMMS	1
		4.3.9 Summary of Subsystems	1
5	Loc	comotion System Design 4	3
J	5.1	Terramechanical Model	
	0.1	5.1.1 Lunar Soil	
		5.1.2 Wheel-soil interaction	
		5.1.3 Static model	
		5.1.4 Dynamic model	
	5.2	Terramechanics Simulations	
		5.2.1 Wheel geometry optimization	
	5.3	Terramechanics results	7
	5.4	Wheels design	9
		5.4.1 Wheel type	2
		5.4.2 Comparative analysis	4
	5.5	Suspension Architecture	5
		5.5.1 Hybrid suspension model	8
6		cussion 7	
	6.1	Terramechanical methodological approach	
	6.2	Wheel geometry optimization logic	
	6.3	Evaluation of wheel concepts	
	6.4	Suspension trade-offs	
	6.5	Integrated system implications	
	6.6	Comparison with state-of-art designs	4

	6.7	Limitations of the analysis	74
	6.8	Implications for lunar exploration architecture	75
	6.9	Synthesis	75
7	Cor	nclusion and future work	7 6
\mathbf{A}	Abl	previations	78
В	\mathbf{AH}	P tables	7 9
		B.0.1 Wheels	79
		B.0.2 Suspension	81
${f L}$	ist	of Figures	
	1	LRV for Apollo 15 mission.	8
	2	Single cylinder configuration	10
	3	Multi-segmented configuration	11
	4	Dual cylinder configuration	11
	5	Rovers' wheel configurations	14
	6	Passive suspension configurations	17
	7	Double A–arm suspension	18
	8	Chariot's suspension	18
	9	Steering configurations	21
	10	Reference traverse scenario	28
	11	Rovers' geometry configurations	30
	12	Pressurized module size	34
	13	Pressurized module 3D view	37
	14	Envelope of the pressurized rover	39
	15	Locomotion system approach flow-chart	43
	16	Diagram of the implemented terramechanical model	44
	17	Soil deformation as a function of the load	46
	18	Variation of the Terzaghi Bearing Capacity factors with the angle ϕ	47
	19	Representation of the wheel in static conditions	48
	20	Representation of the wheel in dynamic conditions	49

21	Compaction Resistance as a function of wheel wiath b and wheel diameter D	53
22	Bulldozing Resistance as a function of wheel width b and wheel diameter D	54
23	Sinkage as a function of wheel width b and wheel diameter D	54
24	Representation of the Pareto-optimal solutions	57
25	Evolution of thrust, resistance and drawbar pull as a function of wheel pressure P_w	58
26	AHP results for wheels	62
27	Types of wheels considered for the preliminary design	64
28	AHP results for suspension	67
29	Hybrid suspension scheme	68
30	Vertical displacement of the sprung mass	71
List	of Tables	
1	Moon - Earth environment comparison	4
2	Technological Challenges on the Moon	6
3	Comparison of pressurized and unpressurised rovers concepts	9
4	Comparative summary of different wheel's designs	15
5	Comparative summary of different suspensions designs	19
6	Classification of requirements based on ECSS Standards	23
7	List of requirements	23
8	Mobility System's requirements	26
9	Configuration trade-off	32
10	Launch vehicles comparison	33
11	Summary of overall dimensions for the pressurized module	36
12	Summary of envelope dimensions	38
13	Summary of subsystems	41
14	Average density as a function of depth range	45
15	Cohesion and friction angle values as a function of depth range	46
16	Equation for normal stress at each contact section	50
17	Soil parameters	52
18	Terramechanical results for $P_w = 11000 \ Pa$	59

19	Wheel's AHP Prioritization Matrix	60
20	Example: wheel's load capacity	61
21	Wheel comparative analysis	64
22	Suspension's AHP Prioritization Matrix	66
23	<i>Traction.</i>	79
24	Adaptability to terrain	79
25	Resistance to lunar dust	80
26	Durability	80
27	AHP Summary for Lunar Rover Wheel Concepts	81
28	$A dapta bility. \dots \dots$	81
29	Maneuverability	81
30	Ride comfort	82
31	Design complexity	82
32	Cost/mass/power demand	82

Abstract

This thesis presents the preliminary design of a mobility system for a pressurized lunar rover. In the context of future long-duration lunar missions, the implementation of a robust and reliable locomotion system is essential to enable the exploration and operations of pressurized rovers across the Moon's challenging terrain. This work starts with a comprehensive overview of lunar environmental conditions and a comparative analysis of current surface mobility platforms. From this basis, mission requirements are derived in accordance with European Cooperation for Space Standardization (ECSS) standards and translated into functional specifications for the mobility subsystem. A terramechanics-based modelling approach is employed to describe the complex interaction between flexible wheels and lunar regolith, considering static and dynamic soil responses. Parametric simulations are used to investigate the influence of wheel geometry on key performance indicators such as sinkage, traction, and driving resistances. Preliminary results demonstrate the trade-offs involved in wheel design and highlight optimal configurations for enhancing mobility efficiency on the Moon. The thesis is further developed to include the initial sizing of the entire locomotion architecture, including drivetrain sizing, suspension and steering mechanisms, in order to provide a fully integrated and mission-ready mobility solution.

Keywords: Lunar exploration, Pressurized rover, Locomotion system design, Terramechanics

Context of the Work

Space It Up! (SIU!) is an initiative involving 33 institutions, including universities, research centers, and industries, aimed at promoting nationwide collaboration for the development and validation of advanced technologies for the exploration and exploitation of space.

The project is structured around 9 research lines (Spokes), each dedicated to a specific topic: new missions for the protection and sustainable development of the planet and planetary exploration missions (Spoke 1), development of technology for the creation of "Digital Twins" (Spoke 2), space remote sensing (Spoke 3), design, development, and qualification of miniaturized high-resolution sensing systems for satellite missions to observe ionizing radiation around the Earth and water reservoirs on the planet (Spoke 4), mitigation of natural and geological risks to the Earth (Spoke 5), investigation of scientific and technological issues within the network of physical processes connecting the Sun to Earth's society (Spoke 6), research on sustainability of human activities to ensure the health of people and the planet (Spoke 7), research and development activities to support future human missions in space (Spoke 8), studies on space travel and human permanence in space and on extraterrestrial celestial bodies, particularly Moon and Mars (Spoke 9).

This thesis is developed within the framework of Spoke 8 - Robotic and human exploration of extraterrestrial habitats, architectures and infrastructures, coordinated by Politecnico di Torino with the contribution of Thales Alenia Space as industrial partner.

This research line focuses on advanced technologies and integrated systems for future human interplanetary exploration missions. It involves several thematic areas, such as space robotics, for autonomous mobility and operations, sensors, for navigation and monitoring, and habitats' design, focusing on structural and ergonomic solutions for long-duration missions.

For more information: https://spaceitup.it/



1 Introduction

Since the early phases of Apollo missions in 1960s, the Moon has been a destination of great interest.

Over the years, several rover concepts for lunar exploration have followed, proposing solutions such as small autonomous rovers up to pressurized rovers capable of carrying laboratories and astronauts' crew. In recent decades, interest in the Moon has strongly re-emerged, as a result of a rapid technological progress and the ambition to create permanent lunar bases for human presence. The purpose of future lunar expeditions is to support human presence for extended periods of time, by using permanent bases not only as scientific incubators, but also as testing grounds for resource utilisation and sustainable habitation technologies, as supported by the Artemis program, which aims to establish a permanent human presence through infrastructures such as the Lunar Gateway and surface habitats [2].

To support such long-term surface operations, pressurized rovers are emerging as essential elements of mission architecture. Pressurized rovers provide safer transportation to areas away from permanent bases, enabling excursions without the constant need for astronauts of space suit. The design of such a complex system presents various technical, operational and environmental challenges. The vehicle shall be able to withstand loads and vibrations in the launch and descent phase, as well as shields against micrometeorites, and a temperature control system for the -130°C to +120°C range [3]. Also, it shall be equipped with a locomotion system that allows transportation over lunar terrain and include life support systems for longer missions.

The following structure is designed to provide a progressive explanation of the challenges and solutions related to the mobility system on the lunar surface. Chapter 2 begins with an introduction to the general background on lunar exploration, describing the environmental characteristics of the Moon and analysing the evolution of surface vehicles, from the first non-pressurized rovers to the more advanced pressurized rovers for crewed missions. Chapter 3 outlines the mission reference scenario, identifying the essential performance and functional requirements that a pressurized rover must fulfill to ensure operational support during long duration missions. Chapter 4 illustrates the preliminary design of the pressurized rover, including the definition of its geometric configuration, mass sizing, subsystems, and integration with launcher constraints. Chapter 5 describes the implementation of the proposed approach, starting with the development of a terramechanics model characterizing wheel-soil interactions under lunar conditions. static model used for the quantification of stress and force distributions culminates in the analysis of the main driving forces, such as resistances and traction. The analysis concludes by presenting the simulations conducted to demonstrate the influence of various parameters on the rover's performance under different scenarios. This chapter concludes with the preliminary identification and analysis of wheels and suspension architectures. Chapter 6 discusses the main results, highlighting the methodological implications, tradeoffs, and consistency with existing designs. Finally, Chapter 7 summarizes the conclusions inherent in the analyses and proposes future developments of the work to improve the reliability of the mobility system for future space missions.

2 General Context

2.1 Lunar environment

In planning a lunar mission, it is essential to study the lunar environment and its differences from the terrestrial environment in order to assess the technical feasibility of the project and define the environmental requirements that have to be met. This comparison is necessary for an in-depth analysis, since all these aspects represent criticalities for the design of habitats and systems on lunar surface. The differences between the terrestrial and lunar environment are shown in Table 1.

Property	Moon	Earth
Mass [kg]	$7.353 \cdot 10^{22}$	$5.976 \cdot 10^{24}$
Radius [km]	1738	6371
Surface area $[km^2]$	$37.9 \cdot 10^{6}$	$510.1\cdot10^6$
Mean density $[g/cm^3]$	3.34	5.517
Gravity at equator $[m/s^2]$	1.62	9.81
Mean surface temperature [°C]	107 (day), -153 (night)	22
Temperature extremes [°C]	-233 to 123	-89 to 58
Atmosphere $[molecules/cm^3]$	$\sim 10^4$	$2.5\cdot 10^{19}$
Heat flow (average) $[mW/m^2]$	~ 29	63
Seismic energy [J/yr]	$2\cdot 10^{10}$	10^{17}
Magnetic field [A/m]	0	24-56

Table 1: Moon - Earth environment comparison.

There are several factors concerning the lunar environmental conditions to pay more attention to, such as extreme temperature fluctuations, low gravity and an extremely thin layer of atmosphere known as exosphere. Besides, other important considerations must be evaluated, such as the ionizing radiations, the micrometeoroids bombardment hazards and the possibility of electrostatic charging of lunar dust [4].

2.1.1 Temperatures

The Moon's surface temperatures show significant variations, with an increase of about 280 kelvin between the minimum temperatures recorded before sunrise and the maximum temperatures reached at lunar noon. Detailed heat flux experiments conducted at the Apollo 15 and 17 landing sites probed the upper few metres of the regolith: these measurements showed daytime highs of about 374 K and pre-dawn lows as low as 92 K.

2.1.2 Meteoroid bombardment

The lunar surface is exposed to a continuous flux of meteorite particles impacting at high velocities, typically between 13 and 18 km/s. The flow intensity is most intense for the

meteoroids coming from the Sun, which have a maximum size of 1 micrometer. Particles coming from the Earth, which have a larger size (> 1 μ m), have a lower intensity but result to be more dangerous, representing a greater potential risk when the lunar surface is facing the direction of the Earth during the orbit. These impacts can generate damage to exposed structures and compromise their integrity, so the use of appropriate protection systems, such as meteorite shielding or coatings with high impact-resistant materials, is essential.

2.1.3 Ionizing radiation

The lunar environment is exposed to different types of radiation, such as solar wind, solar flare particles and galactic cosmic rays. These particles, consisting of protons and electrons with heavier nuclei, have the capacity to penetrate the ground up to tens of centimeters, depending on their energy.

- Solar wind: flux of ionized plasma emitted by the Sun that propagates creating magnetic field lines. This phenomenon is one of the secondary factors in surface erosion and causes sputtering and changes in soil particle composition.
- Solar flare particles: these particles, which originate from solar flare events, are also called solar cosmic rays (SCRs). The intensity of the flux, after rapidly increasing following a solar flare, decays at a rate inversely proportional to the energy of the particles. Long-term exposure of the vehicle to these fluxes can cause significant damage to exposed surfaces and electronic components. While these particles may represent a potential hazard to the rover's integrity, they are less of a concern than galactic cosmic rays, due to their relatively low energy.
- Galactic cosmic rays: they may represent a problem due to the high energy of the particles, even though the frequency of the flux is low ($\sim 4~protons/cm^2~s$). High-level energy of soft x-rays and ultraviolet rays can affect surface coatings and optics through their elastic and inelastic scattering processes.

2.1.4 Dust

The particles of the lunar soil, called regolith, have a size between 45 and 100 μm . These grains are highly abrasive and could erode several mechanical mechanisms and optics components. Besides, lunar dust has a low electrical conductivity and dielectric losses, and this can lead to an accumulation of electrostatic charge under ultraviolet irradiation. When the rover is moving across the Moon, clouds of electrostatic dust may arise and reach heights of over 2 meters.

The lunar environment presents specific conditions that necessitate a thorough evaluation of the technological challenges that will be encountered. In Table 2 a comprehensive summary is shown.

Table 2: Technological Challenges on the Moon.

Environmental	Engineering/Operational	Technological
Factor	Implications	Response
Extreme temperature range	Overheating/overfreezing	Insulation, suitable materials
Micrometeroids bombardment	High-speed impacts	Impact shielding, structural reinforcement
Radiation	Surface and electronics damage, biological hazard	Radiation shielding
Dust	Infiltration, electrostatic charging, abrasion	Dust coatings, sealed design
Vacuum	Outgassing, evaporation of lubricant	Compatible materials, dry lubricants
Low gravity	Mobility issues, crew health hazard	Adaptive suspension, human physiological mitigation strategies

2.2 Surface exploration vehicles - State of art

Lunar exploration vehicles are robotic systems designed especially for mapping and investigation of the lunar surface. The rovers currently in use are small-scale and unmanned and have been developed for short-duration missions. These systems are designed to explore the terrain typically found near the landing site. They carry out on-site analyses to determine the mineralogical and chemical composition of the regolith and obtain data that can be used to trace the geological history of the lunar surface. The vehicles, designed to explore the lunar environment over distances of a few hundred metres or kilometres depending on mission constraints and terrain complexity, implement specialised mobility systems and autonomous navigation. However, there has recently been a growing interest in developing pressurized rovers to extend mission range and duration, and most importantly, to provide a safe and habitable environment for astronauts. These two types of rovers differ not only in their intended operational objectives, but also in their design implications, specifically concerning energy autonomy, subsystem redundancy and the integration of life support systems.

2.2.1 Unpressurized rovers

Unpressurized rovers are surface mobility platforms designed for short traverses on the lunar surface. Compared to the several types of rovers used in planetary exploration, they are among the most developed and widely employed due to their simple design, light weight and adaptability to many different mission scenarios and terrains.

Unpressurized rovers are typically classified into two major categories based on the presence or absence of an onboard crew:

Unmanned unpressurized rovers These robotic systems can be operated remotely from Earth or via pre-programmed autonomy. They are dedicated to exploration, scientific operations and terrain reconnaissance, and generally present the following characteristics:

- No life support systems that require mass and power;
- Long-duration missions, particularly on Mars, when powered by solar and nuclear sources;
- Scientific payloads, such as cameras, spectrometers, drills, environmental sensors and seismometers;
- Mobility systems designed for extraterrestrial terrain, e.g. rocker-bogie suspension and optimised traction wheels.

Key examples include Lunokhod 1 and 2 (1970–1973), the first robotic lunar rovers to be remotely controlled from Earth and equipped with cameras, soil analysers and spectrometer [5]. Other notable missions include NASA's rovers INSPIRE [6] and Endurance [7], representing more recent developments in planetary surface exploration.

Manned unpressurized rovers These vehicles are operated directly by astronauts when they are on the surface of an extraterrestrial body. They primarily serve as local mobility vehicles, enabling crews to extend their exploration range. As these systems do not provide environmental isolation from the lunar surface or an enclosed pressurized cabin, the astronauts are required to wear a full Extravehicular Mobility Unit (EMU) for the entire operation.

The design of manned rovers must consider ingress and egress in bulky suits, resistance to dust contamination and the safe navigation of lunar slopes and obstacles. Unlike unmanned rovers, these systems must meet strict safety and reliability standards in order to support human life in harsh extraterrestrial environments.

The most representative example is the Lunar Roving Vehicle (LRV), developed by NASA for Apollo 15, 16 and 17 missions. This vehicle was a four-wheeled, battery-powered electric rover weighing 210 kg with a maximum range of approximately 92 km under ideal conditions. It featured passive suspension and mesh wheels for lunar regolith, carrying two astronauts plus equipment [8].

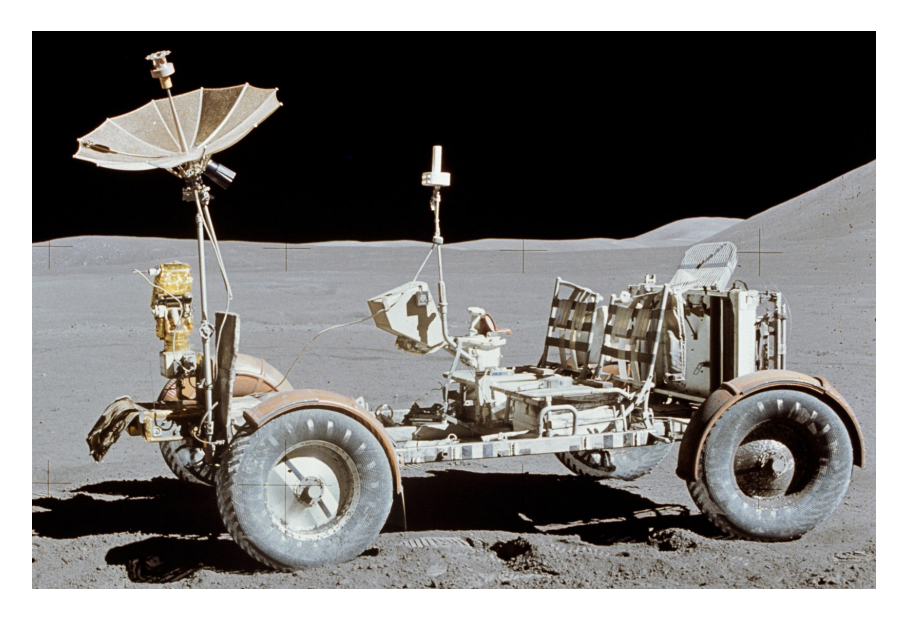


Figure 1: LRV for Apollo 15 mission¹.

2.2.2 Pressurized rovers

A pressurized rover allows missions to be conducted over an extended range, with both a comfortable environment and an improved radiation protection for the crew. Over the past few decades, various pressurized rover designs have been developed to support the sustained exploration of non-terrestrial surfaces. These designs differ from one another in terms of levels of pressurization, habitability and the number of crew (typically from two to four astronauts), as well as mission duration (from short to several weeks traverses). Key architectural differences include rigid, deployable and hybrid pressure vessels, Environmental Control and Life Support Systems (ECLSS) for human habitability, modular power and thermal control systems, and mobility platforms designed to operate in low gravity and extreme environmental conditions. A detailed analysis of the key subsystems required for the design and operation of a pressurized rover will be presented in the following sections.

Examples of this category include NASA's Space Exploration Vehicle (SEV) [9], which could support 14-day lunar sorties, and the JAXA-Toyota Lunar Cruiser, which is designed for longer stays on planetary surfaces and features fuel cell electric propulsion and autonomous driving capabilities [10]. These platforms are essential for planetary surface operations, as they facilitate intra-site mobility, the deployment of scientific payloads, and the safe habitation of crews in support of long-duration missions under programs such as Artemis and future lunar exploration initiatives.

A comparison between the main characteristics of the existing lunar rovers is presented in Table 3, considering their roles, performance, benefits and limitations.

¹Image from https://nssdc.gsfc.nasa.gov/planetary/lunar/apollo_lrv.html (Accessed on 05 Mar 2025).

Table 3: Comparison of pressurized and unpressurised rovers concepts.

				Mass	Max	Range			
Vehicle	\mathbf{Type}	Crew Size	Size	$[ext{tons}]$	${ m Speed} \ [{ m km/h}]$	[km]	Benefits	Limitations	Ref .
NOMAD	Unpressurized	0	$2.4 \text{ m} \times 2.4 \text{ m} \times 2.4 \text{ m} \times 2.4 \text{ m}$ $\times 2.4 \text{ m}$	0.77	1.8	>200	Automatic obstacle avoidance	Only for terrestrial environment	[11]
Dual Mode Lunar Roving Vehicle	Unpressurized	2	$3.5~\mathrm{m} \times 3~\mathrm{m}$		∞		Teleoperated between missions	Radioisotope in close proximity to crew	[12]
Rover First	Pressurized	2	$4.1~\mathrm{m}\times2.6~\mathrm{m}$	4.3	1	80	No lander needed	Slow speed and limited range	[13]
USRA (Creel) Pressurized	Pressurized	4	$7 \text{ m} \times 3 \text{ m}$	6.2	18	200	Wheels designed for traction and shock absorption	Skid steering ineffi- cient	[14]
$\begin{array}{c} \mathrm{USRA} \\ (Bhardwaj) \end{array}$	Pressurized	4	$11 \text{ m} \times 4 \text{ m}$	2	29.4	2000	Ideal for movement in loose soil	Planetary friction drive power limited	[15]
Lunar Polar Rover	Pressurized	ಣ		80.9	20	100	Concept provides for drilling & digging equipment	Limited range	[16]
Habot	Pressurized	9	5 m dia. (each module)	10 (each module)			Provides mobile base and unit clustering	Complex walking mechanism	[17]
MORPHLAB	Pressurized	4	4 m dia. each habitat	3.7 each unit		1000	High modularity and redundancy	Relies heavily on advanced autonomous technology	[18]

2.3 Pressurized rover configurations - State of art

Examining more closely the evolution of pressurized rovers, the design phase requires, among other factors, the definition of the geometric configuration, which has a decisive impact on structural and mobility performance. In recent decades, various geometric solutions have been proposed, each with specific advantages and limitations in terms of habitable volume available, ease of transport and deployment and adaptability to different operational scenario. Among the various configurations, three of these are discussed in detail below: the single cylinder configuration, the multi-segmented configuration and the dual cylinder configuration [15].

2.3.1 Single cylinder configuration

This single cylinder configuration is the simplest and most intuitive solution, featuring an elongated pressurized body and a conventional chassis. The main benefits of this architecture are its relatively low centre of gravity, which improves the rover's dynamic stability during traversal, and its regular shape, which allows for a linear interior layout and facilitates the integration of life support systems. A long overall length can reduce manoeuvrability on rough terrain and cause significant stress on the chassis, especially on uneven or sloping ground. Furthermore, modularity is reduced compared to more complex architectures.

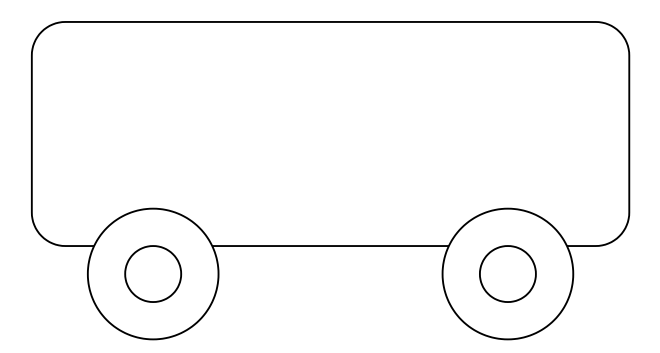


Figure 2: Single cylinder configuration.

2.3.2 Multi-segmented configuration

The multi-segmented configuration adopts a modular approach, based on the use of multiple pressurized volumes connected to each other and mounted on a frame that can be rigid or articulated. In this architecture, the modules can be sized and connected in varying numbers depending on the mission, allowing for a balance between living space and overall mass. Segmentation allows for better distribution of loads along the structure and greater adaptability to the terrain, as the multi-jointed frame reduces stress and increases manoeuvrability. However, the multiplication of pressurized joints introduces critical issues of reliability and construction complexity, as each connection must guarantee mechanical strength and the division of interior spaces can reduce living efficiency compared to more regular single volumes.

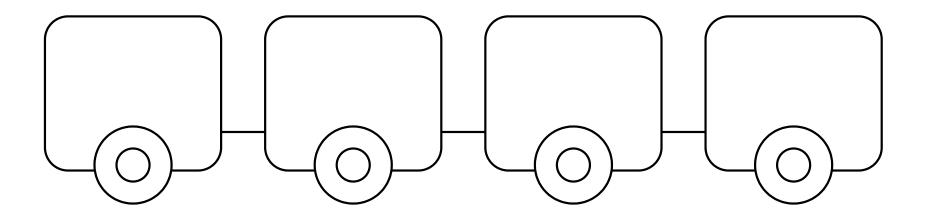


Figure 3: Multi-segmented configuration.

2.3.3 Dual cylinder configuration

The double-cylinder configuration represents a compromise between the structural advantages of spheres and the internal functionality of cylinders. Two cylindrical modules are connected in a single structure by an extensible membrane, allowing for a more balanced distribution of loads and more efficient use of internal space. The presence of two pressurized modules ensures greater modularity: one of the cylinders can be dedicated to habitable quarters and the other to operational or logistical functions. The main disadvantage is the complexity of construction and the increase in the number of critical connections, which require robust structural solutions to maintain reliability and pressurized integrity.

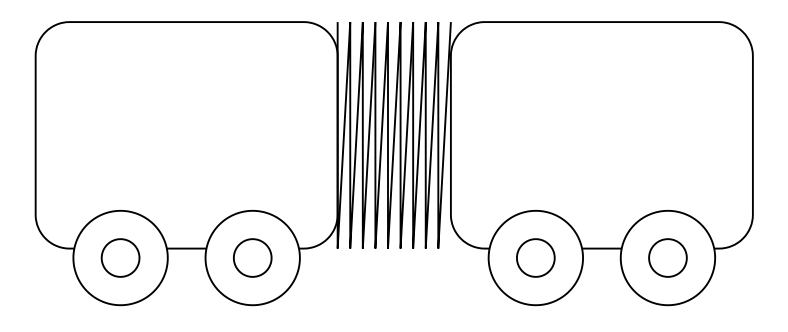


Figure 4: Dual cylinder configuration.

2.4 Mobility Systems - State of art

Mobility technologies are considered one of the key subsystems of lunar rovers and can directly impact the range, safety and scientific or operational output of surface missions. Compared to static landers, rovers enable the exploration of a greater variety of locations and provide access to different geological formations, while also performing logistical tasks such as returning samples or transporting resources. Designing a mobility system for the Moon is challenging due to its environmental conditions: low gravity, loose regolith covering the surface, large daytime-nighttime thermal excursions and the lack of an atmosphere. These factors impose severe requirements for wheel design, traction control, structural strength and dust mitigation methods. A lunar mobility system consists of wheels (or alternative locomotion equipment), suspension and steering systems, drive motors and transmission components, as well as the control systems for traction and navigation. The main objective is to provide sufficient contact with the ground and traction on rough terrain to prevent sinking and energy loss.

Wheels Wheels are designed as non-pneumatic structures since pressurized tyres cannot operate in a vacuum or at cryogenic temperatures: not only would the material itself deteriorate under radiation and temperature extremes, but any puncture in a vacuum environment would immediately render a manned rover immobile, constituting a disastrous single-point failure [19]. Across the decades, the most effective solutions have been compliant metallic wheels: these designs permit to achieve low stiffness and to avoid sinkage, while having high endurance against dust abrasion and thermal cycling.

These challenges were initially addressed by defining the design of the wheels for the Lunakhod rovers. Each Lunokhod's wheels consisted of wire mesh tyres on lightweight rims, supported by sixteen spokes and fitted with metal grousers to provide traction (Figure 5a). The decision to use wire mesh with grousers was intentional: the mesh increased the wheel's compliance and elasticity, enabling the deformation across rocks and the distribution of the load over the surface, while the grousers provided traction by generating shear with the soil. This design was created in response to the fundamental issue of travelling over uneven and loose surfaces, where pure frictional contact is insufficient to generate thrust.

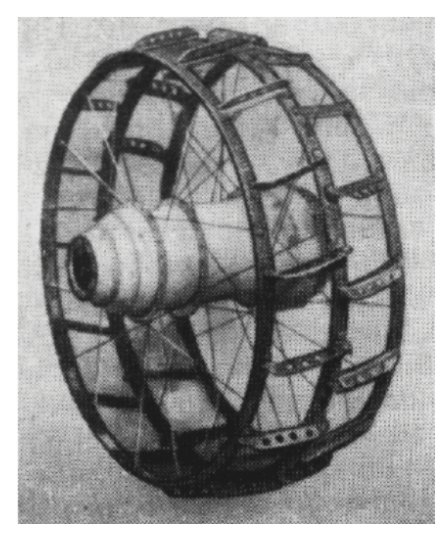
NASA's development of the Apollo LRV was inspired by the same goals but was designed to meet the requirements of a manned mission. The wheels were fabricated using a zinc-coated, woven piano wire mesh over a robust aluminium hub, and were supported by an internal titanium bump stop to limit over-deflection, while the titanium grousers covered the 50% of the circumference (Figure 5b). As previously mentioned, this configuration enabled to distribute the load and generate traction simultaneously. Due to the elastic properties of the wire mesh, the loaded wheel mesh acted as a vibration damper while the rover was travelling at higher speeds, thereby improving ride comfort for the astronauts. However, testing revealed a fatigue issue: repeated strikes against obstacles led to local wire failure. A significant engineering accomplishment was represented by the LVR wheels, with their usable mass, durability, and safety for human missions.

Also, more advanced compliant wheel concepts were explored beyond traditional wire mesh designs, such as the hoop spring and the spiral spring wheel. The hoop spring wheel consisted of a titanium outer rim supported by multiple hoop springs connected to a rigid hub (Figure 5c). This configuration produced a large, uniform contact patch and distributed loads locally. Testing revealed two disadvantages: extreme vibration, or 'flutter', occurred at critical velocities, and the hoop springs experienced reverse bending fatigue when crossing sharp rocks. This resulted in the development of ellipse spring wheels, where radial elliptical elements connected the hub with the tread. These elements influenced one another to provide a variable stiffness mechanism: for minor loads, one or two elements supported the load. As the deflection increased, adjacent elements came into action, distributing stresses over an increasing number of supports. This resulted in a more material-efficient wheel, providing a lighter alternative to hoop spring designs. Another version was the spiral spring wheel, which used bi-tangent semicircular springs connected to a central hub and a deformable tread (Figure 5d). Unlike the elliptical spring concept, its stiffness curve was linear with load, providing predictable but less compliant performance.

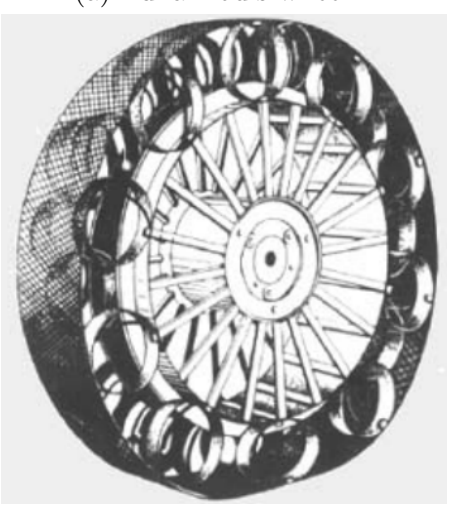
Moving to more recent innovation, for the INTREPID rover concept by NASA a springtire design has been developed (Figure 5e). This airless compliant tire consisted of several coiled steel wires interwoven into a flexible mesh, resulting in much greater payload capacity and adaptability. These wheels demonstrated a high performance on lunar soil simulation, although their efficiency is highly dependent on the choice of material, as the meshes of spring must be ductile to avoid the risk of brittle fracture at cryogenic temperatures on the moon.

One of the novel concept lunar rover wheel designs is the Venturi wheel, whose purpose is to overcome loose regolith challenges. The wheel, through on a new super-elastic material and cable-spring reinforced design, is both highly compliant and durable. It incorporates 192 stainless steel cables connecting the inner rim with the tread, placed in multiple rows and angles for maximum transmission of force and traction. The cables extend at the contact patch to conform to the lunar surface and contract at the top section, enabling the wheel to firmly grip and maintain its shape for each rotation. The tread consists of stainless steel blades secured by the unique elastic alloy, maintaining great flexibility even at lunar cryogenic temperatures.

Latest research is focusing on composite flexible wheels for their application on Pressurized Lunar Rovers. These concepts have the potential for intelligent behaviour: as the wheel flexes, it increases traction on soft soil and stiffens on hard surfaces to decrease rolling resistance. The general concept remains the same in all cases: the wheels must be lightweight and compliant, resistant to fatigue, and able to generate sufficient traction without the use of rubber or internal pressure.



(a) Lunakhod's wheel



(c) Hoop spring wheel



(e) INTREPID's wheel



(b) LRV's wheel



(d) Spiral spring wheel



(f) Venturi's wheel

Figure 5: Rovers' wheel configurations.

Table 4: Comparative summary of different wheel's designs.

Vehicle/Wheel Materials Type	Materials	Compliance	Traction Method	Advantages	Limitations
Lunokhod	Al wire mesh + grousers	Elastic	Grousers shear	Lightweight, proven in regolith	Limited ride comfort
Apollo LRV	Woven zinc-coated steel wire mesh + Ti chevrons + Al hub	Elastic	Shear failure	Ride comfort, stabil- ity, flotation	Wire fatigue
Hoop Spring	Ti hoops + Al hub	Elastic	Metal friction	Large contact patch	Flutter, fatigue
Ellipse Spring	Radial elliptical spring steel	Variable	Shear/friction	Efficient, lightweight	Complexity
Spiral Spring	Bi-tangent spring steel	Constant	Shear/friction	Predictable stiffness	Less adaptive
Intrepid	Coil spring mesh	Elastic	Shear/friction	High mobility, durable	Cryogenic ductility
Venturi	Stainless steel ca- bles + stainless steel blades and super-elastic alloy tread	Elastic	Cable expansion and contraction	Puncture-proof, radiation resistant, cryogenic resilience, atmosphere independent	Complexity, no space heritage

Suspension Suspension system is a critical subsystem of planetary rovers, since it directly influences mobility, stability, ride quality, and structural loads. Unlike ground vehicles, rover suspensions must provide high reliability at reduced gravity, irregular terrain, and mass or volume constraints usually in an unmaintainable environment. Several kinematic architectures have been invented and tested throughout the years, depending on the specifications of the rover. As a result, suspension designs have followed very different paths depending on whether the rover is unmanned, where simplicity and reliability are the primary needs, or manned and pressurized, where ride comfort, safety, and flexibility become dominant requirements.

The first category includes purely passive suspensions, based on kinematic linkages (Figure 6). Designed to keep all the wheels in contact with the ground without the use of springs or dampers, these suspensions are ideal for unmanned rovers, where simplicity, reliability and weight efficiency are more important than ride comfort. The Rockerbogie suspension represents a well-known example, first developed with NASA's Mars Pathfinder mission and subsequently applied to all Mars rovers, from Sojourner to Curiosity and Perseverance. It relies on two extended rocker arms carrying the front and middle wheels, which are joined by a differential that equalizes motion between the two sides, and two bogies carrying the rear wheels. The design of rocker—bogie suspension allows a rover to traverse objects as high as 1.2 times the wheels diameter, while evenly distributing load, without requiring active components.

The ExoMars mobility studies examined alternatives such as the RCL-C (Figure 6a), RCL-D (Figure 6b) and CRAB (Figure 6c) concepts, which involved pantograph linkages that offered good wheel contact and obstacle crossing. However, these were limited by suspension 'hang-up' on obstacles and the added complexity of extra linkages. The RCL-E mitigated these issues by using an independent transverse bogie with the removal of the central differential but still it experienced stability problems on slopes. To further enhance stability, two new passive geometries were created through these designs: the 3-bogie layout, which eliminated pantographs and fixed wheel supports to beams, thereby offering a lightweight, simple, yet stable arrangement (Figure 6e); the V-bogie, which presented pantograph arms into an inverted V, enhancing downslope wheel reaction forces and static stability (Figure 6f). These passive linkage systems have become the reference for unmanned exploration, since they are considered mechanically reliable and fault-tolerant, with few or no moving components. The main disadvantage to these systems lies in the damping; it transmits all shocks directly to the chassis, acceptable for a robotic platform but not for human transport.

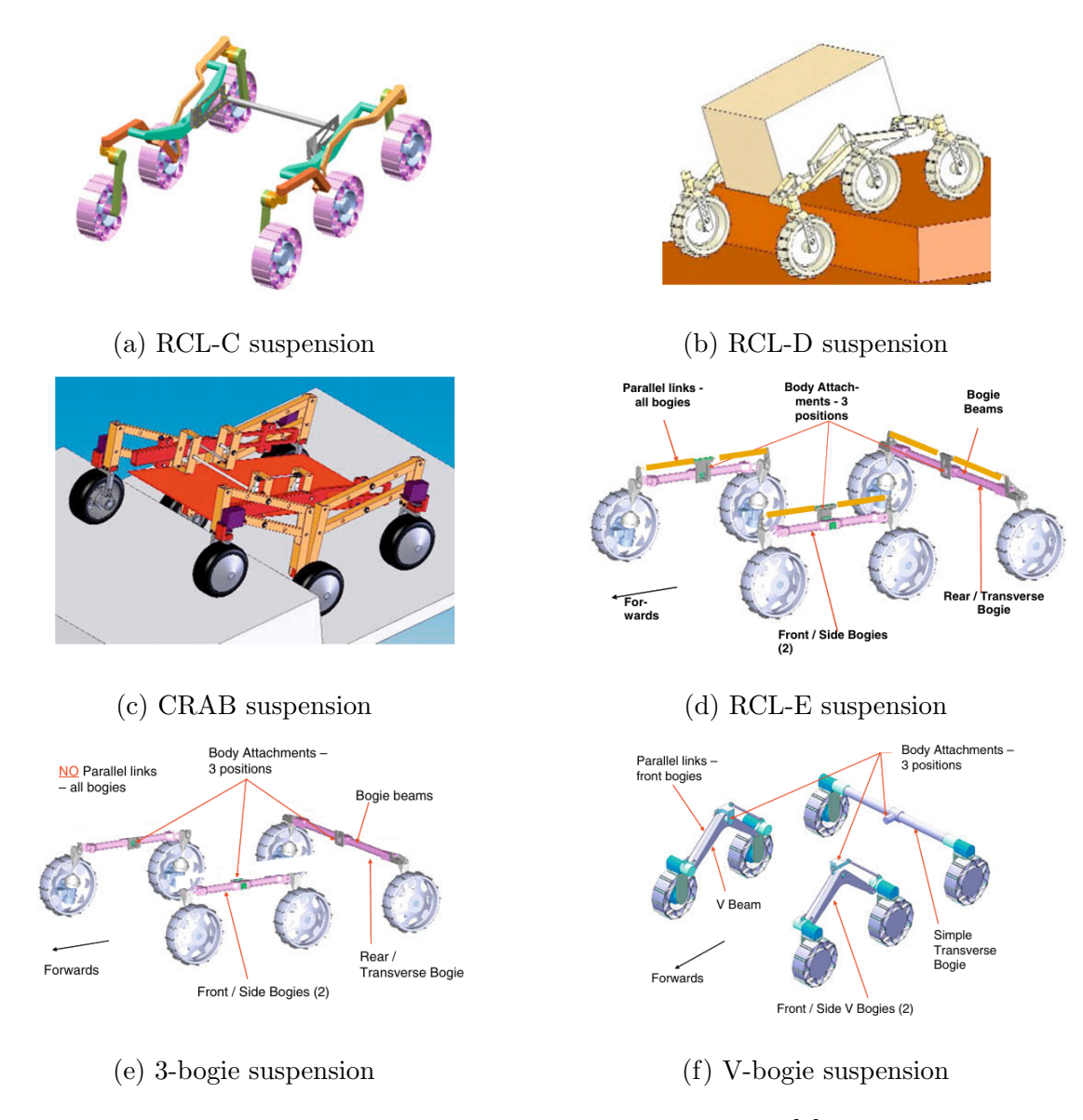


Figure 6: Passive suspension configurations [1].

When considering crew comfort and safety, the addition of independent suspensions with elastic members and dampers becomes necessary. In a more sophisticated designs for long-duration missions, like NASA's Lunar Pressurized Rover (LPR), a double A-arm suspension was selected (Figure 7). Equal-length upper and lower arms maintained wheel camber virtually invariant, while the telescopic spring-damper absorbers ensured that the effects of impact dissipated as heat rather than resulting in excessive rebound. Also, the materials were carefully selected: thin-walled tubular steel for the arms, aluminium for the kingpins and steel shafts for the wheels. Overall, this design achieved a balance of high mobility, structural simplicity and reliability.

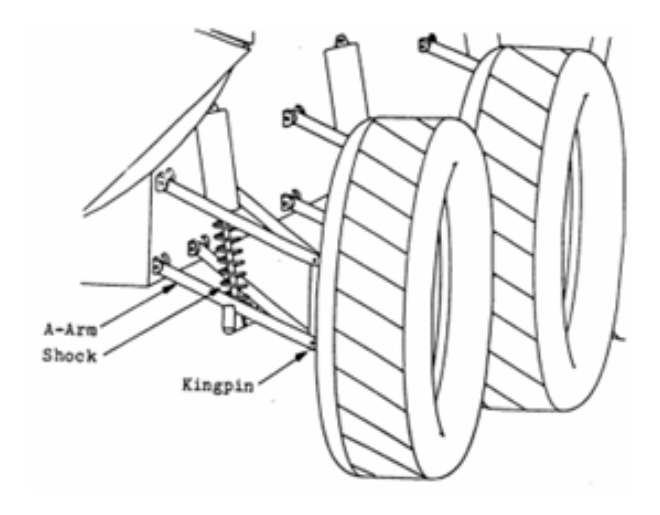


Figure 7: Double A–arm suspension.

The most sophisticated developments involve active or semi-active suspensions, that combine passive compliance with programmable actuation to optimise performance according to mission requirements and terrain. These systems have been extensively researched in NASA's Lunar Electric Rover (LER) and Chariot project, where a series-elastic active suspension was introduced. Each wheel module incorporated a double control arm with coil-over spring—damper shocks (the passive element), in series with an actuated ball-screw mechanism (the active element) (Figure 8). The control system included position and compliance modes. In position control, the system actively maintained the pitch, roll and ride height of the chassis. In compliance control, the actuators applied 'virtual springs' based on Hooke's law, extending the range of passive suspension and limiting low-frequency loads.

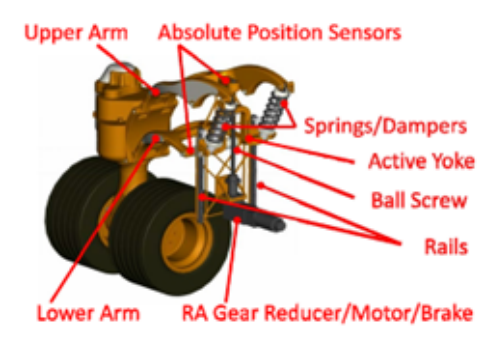


Figure 8: Chariot's suspension.

Rover suspension design is currently proceeding in this direction, with hybrid architectures that use lightweight materials, efficient actuators, and advanced control algorithms to achieve the robustness of passive systems combined with the adaptability of an active system. In Table 5, a summary of the main suspension technologies is shown.

Table 5: Comparative summary of different suspensions designs.

Suspension Type	Technology	Advantages	Limitations
Rocker-bogie	Passive linkages + dif- ferential	High obstacle clearance, reliable	No shock absorption, imited ride comfort
RCL/CRAB/3-bogie/V-bogie	Pantograph linkages, passive	Low mass, 6-wheel contact, differential load sharing	Limited slope stability
Double A-arm	Passive, spring-damper	Large clearance, independent wheels, good comfort	Added complexity, more joints
Series-elastic active + passive	Active actuators + passive shocks	Adjustable height, slope and docking leveling	Increased weight, power demand, complexity

Steering Unlike terrestrial vehicles, planetary rovers need to operate under conditions demanding superior manoeuvrability, high traction, and fail-safe redundancy. Therefore, the choice of steering architecture involves making an informed trade-off between geometrical principles, terrain compatibility and mission scenario.

Skid steering (Figure 9a) presents a rotation by changing the speed of the wheels on either side. The wheels are fixed to the chassis, with the turn is produced with lateral slip. The geometry is simple: a symmetric vehicle can turn around its geometric centre, and zero turning radius point turns are generated. This is advantageous on restricted manoeuvring area, but it requires a lot of energy. The Lunokhod I represents an example of this concept: an eight-wheeled rover that used skid steering exclusively and could rotate about its centre of mass. The Marsokhod operated similarly, with a six-wheel skid steering system. The reduction in moving parts and mechanical complication with skid steering is beneficial; however, loss of traction in a turn can severely affect capability on slopes and loose terrain.

Ackermann steering (Figure 9b), initially designed for terrestrial vehicles, involves inner and outer wheels that share a common turning centre. The aim of implementing the Ackermann steering is to minimise slip when turning and to produce smoother and more efficient steering at medium to high speeds, requiring precise linkages and dedicated actuators. The Apollo LRV was equipped with front and rear Ackermann steering, with each set of wheels controlled by a separate actuator via linkages [20]. This double steering system allowed for more compact manoeuvres, but the minimum turning radius was still approximately equal to the length of the vehicle. This was acceptable for the Apollo missions, as the astronauts could react quickly if a hazard was detected and to intervene physically if the rover became stuck. However, for unmanned rovers, this reliance on human response and relatively large turning radius makes Ackermann steering less suitable.

Articulated steering (Figure 9c) removes steering joints at the wheels. The rover chassis is divided into two or more sections connected by hinged joints and articulation can also incorporate roll or pitch axes so that the vehicle dynamically adjusts to uneven terrain.

Independent steering (Figure 9d) provides each wheel with its own actuator. This arrangement allows not just Ackermann-like behaviour but also special modes such as crab steering (all wheels set parallel so the vehicle will travel sideways) or coordinated point turns with minimal slip. Each wheel module is a independently driven and steered unit that must be well electronically coordinated to avoid actuator conflict.

In the near future, manned rovers will increasingly use independent, all-wheel steering with advanced electronic coordination, providing superior capability of manoeuvrability during operations on Moon surface.

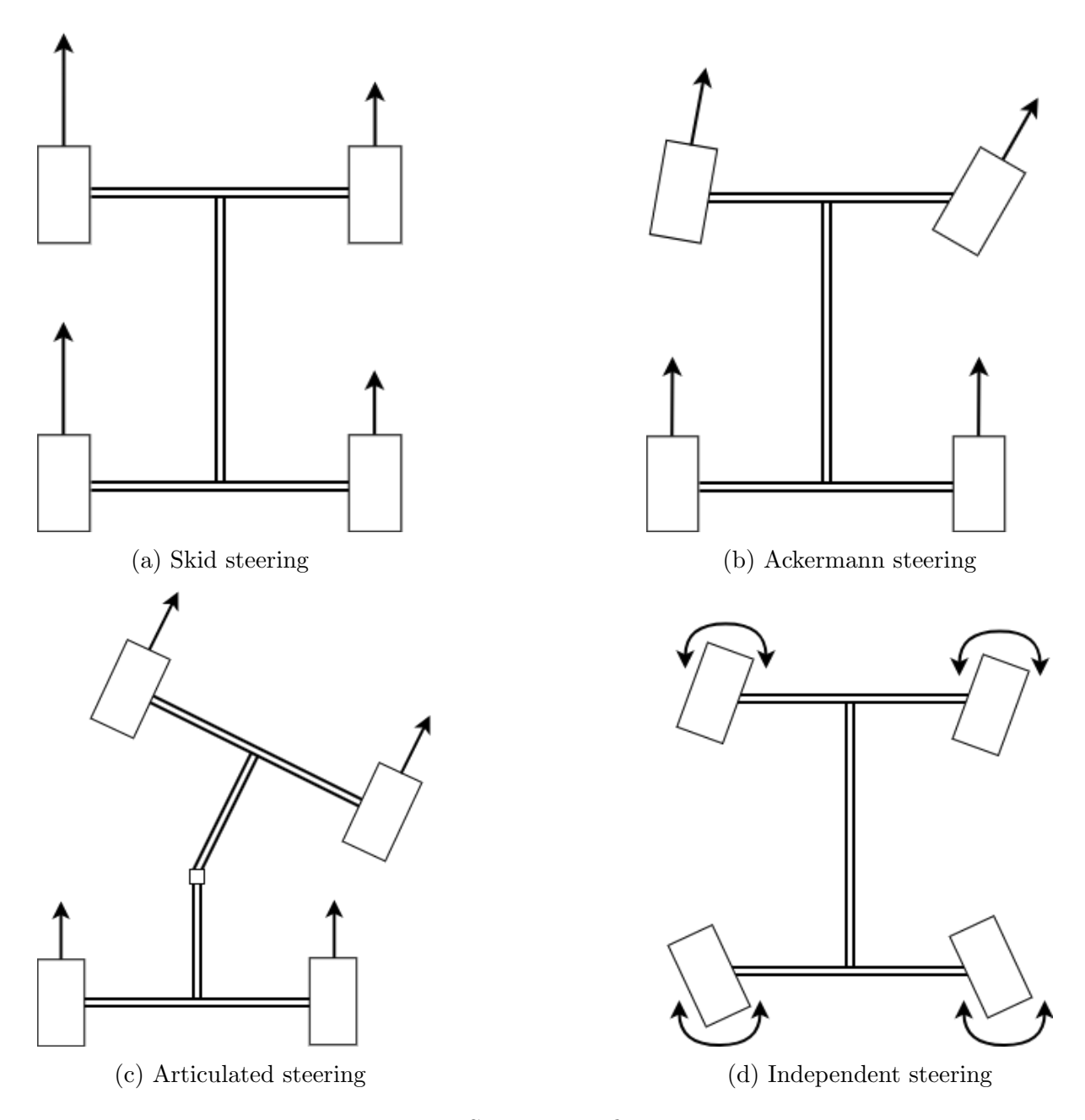


Figure 9: Steering configurations.

To summarize, the state of art suggest that compliant, non-pneumatic wheels and passive suspensions ensure durability and efficiency, as demonstrated on several missions. On the other hand, opportunities for innovation in the development of rovers for use on the Moon have included active suspension, hybrid locomotion systems and modern energy solutions to support future ambitions to inhabit and explore the lunar surface.

3 Mission and Requirements

3.1 Mission Overview

To ensure a sustained human presence on the Moon, it is crucial to define a coherent and operationally realistic mission framework. The focus is on long-range operational domains, in regions that lie outside the protective and logistical perimeter of the primary lunar habitat and present challenges in terms of access, support and sustainability.

In this context, the use of a pressurised lunar rover is fundamental for the mission success. Implementing this kind of vehicle would enable crew members to explore the lunar surface on missions lasting up to several hours and covering wider distance.

The expanded operational range allows geological sites of great interest to be reached, where investigations can support two primary activities:

• Science and sample collection

The Moon represents a unique environment in which a wide range of scientific experiments can be conducted. Unlike Earth, the stratification of the Moon's soil can provide evidence of galactic activity and solar behaviour dating back 4 billion years. In addition, the lack of atmosphere, the nearly aseismic ground surface and the radio-quiet zones on the farside would allow deep-space observations that would not be possible from Earth or from Low Earth Orbit (LEO).

• In Situ Resource Utilization (ISRU)

One of the strategic requirements for implementing permanent infrastructure on the lunar surface is ISRU. The production of oxygen for life support systems and hydrogen for propulsion applications plays a central role. Using these resources locally as an oxidiser and fuel would substantially reduce the mass that needs to be launched from Earth's surface, which is currently dominated by propellants for both reaching LEO and interplanetary or deep-space missions. In the context of future extended-duration missions, using mineral resources on the lunar surface would be crucial for ensuring operational sustainability. Exploiting metals such as aluminium and titanium for constructing and maintaining habitats, as well as semiconductor materials such as silicon, would reduce dependence on terrestrial logistics. Also, uranium is of particular interest as it could be used for the construction of nuclear power systems and ensure a continuous energy supply [21].

3.2 Requirements

A comprehensive definition of requirements is essential to successfully perform the mission. During the first steps high-level requirements are identified through an ongoing process, involving multiple refinements. These are derived from a careful analysis of the Statement of Work (SoW), which contributes to the identification of the mission objectives and constraints. Based on ECSS Standards [22], a categorisation of requirements is formulated, following the classification shown in Table 6.

 ${\bf Table~6:~\it Classification~of~requirements~based~on~\it ECSS~Standards.}$

Typology	Abbreviation
Mission	MISS
Environmental	ENV
Design	DES
Functional	FUN
Operational	OPS
Configuration	CON
Interface	INT
Physical	PHY
Human Factor	HUM
Product Assurance	PA

Table 7: List of requirements.

	HIGH LEVEL REQU	JIREMENTS LIST	
ID	Requirement name	Description	Ref.
	MISSION REQ	UIREMENTS	•
LPR-MISS-010	Nominal operational radius (lunar day)	The rover shall have a nominal operational radius of 150 km per mission (lunar day)	[15]
LPR-MISS-020	Nominal operational radius (lunar night)	The rover shall have a nominal operational radius of 100 km for lunar night operations	[15]
LPR-MISS-030	Nominal operational time	The rover shall provide an operational mission duration of up to 20 hours	
LPR-MISS-040	Extended operational time	The rover shall provide an extended operational mission duration of up to 3 days	
LPR-MISS-050	Nominal crew	The rover shall be able to support a nominal crew of 2	
	ENVIRONMENTAL	REQUIREMENTS	
LPR-ENV-010	Lunar gravity resistance	The rover's structure shall withstand lunar gravity of 1.62 m/s^2	[15]
LPR-ENV-020	Lunar dust mitigation	The rover shall include protective measures to prevent lunar dust	

LPR-ENV-030	Protection from solar and galactic radiation and micrometeoroids	The rover shall be equipped with radiation shielding to protect occupants from solar and galactic radiation, and micrometeoroids		
LPR-ENV-040	Thermal resistance	The rover shall withstand lunar temperature variations from +120°C to -150 °C	[3]	
	DESIGN REQU	JIREMENTS		
LPR-DES-010	Lunar dust resistance	The rover shall have a dust-resistant design and employ systems to protect sensitive equipment	[15]	
LPR-DES-020	Modularity	The rover shall incorporate modular design approach to allow flexible adaptation across mission types and duration		
	OPERATIONAL R	EQUIREMENTS		
LPR-OPS-020	Emergency one-time range	The rover shall provide emergency travel capacity of 2000 km for a crew of 2 people	[15],[3]	
LPR-OPS-030	Emergency with no range	The rover shall be able to support a crew of 2 in an emergency without a specific range requirement		
LPR-OPS-040	Obstacles detection and avoidance	The rover shall employ integrated on board sensors for obstacle detection and avoidance		
LPR-OPS-050	Emergency stop command	The rover shall stop moving within a maximum time period of 2 seconds in case of emergency stop command		
LPR-OPS-060	Idle mode	The rover shall ignore all commands related to motion when in idle mode		
	FUNCTIONAL REQUIREMENTS			
LPR-FUN-010	Redundancy	The modularity of the rover shall enhance reliability by allowing interchangeable modules and redundancy		

LPR-FUN-020	Insulation	The rover shall feature thermal control systems to manage internal and external temperature control		
	INTERFACE RE	_		
LPR-INT-010	Communication System	The rover shall incorporate a communication system for direct communication with Earth and lunar EVA operations, including an omnidirectional antenna for local communication		
LPR-INT-020	Common Interfaces	The rover shall utilize standardized interfaces to ensure compatibility and ease of module replacement across different mission profiles and vehicle types		
LPR-INT-030	Docking fixture, robotic arm and storage compartments	The rover shall include docking fixtures compatible with lunar base airlocks, robotic arms for sample collection and handling, and storage compartments for tools and samples		
LPR-INT-040	Power distribution	The rover shall be equipped with an electrical power distribution system that can support all its subsystems		
	CONFIGURATION	REQUIREMENTS		
LPR-CON-010	Primary power source	The rover shall have a primary power source providing continuous $P_{tot} < 10 \ kW$ of power		
LPR-CON-020	Secondary power source	The rover shall include secondary power source to provide an auxiliary power supply of $P_{aux} < 5 \ kW$		
PHYSICAL REQUIREMENTS				
LPR-PHY-010	Compatible airlock	The rover shall include an airlock compatible with lunar habitat modules for EVA access	[15]	
	HUMAN FACTOR REQUIREMENTS			

	ECLSS functions	The rover shall be equipped		
		with Environmental Control	[15]	
		and Life Support System		
		(ECLSS) functions, including		
LPR-HUM-010		carbon dioxide removal,		
		humidity control, atmosphere		
		monitoring, and temperature		
		control		
	Maximum radiation dose	An individual crewmember's		
		total career effective radiation		
LPR-HUM-020		dose due to spaceflight	[23]	
		radiation exposure shall be		
		less than $600 \ mSv$.		
	PRODUCT ASSURANCE REQUIREMENTS			
	Health Management System	The rover shall incorporate		
		health management systems to		
LPR-PA-010		monitor and ensure the		
		reliability of subsystems across		
		extended mission durations		

Once the mission objectives and the high-level requirements related to them are clearly identified, the focus is directed to a more specific analysis of requirements related to the mobility system. This system plays an essential role in the execution of operations on the lunar surface, including ensuring locomotion, terrain adaptability and vehicle stability. To support these functions efficiently, it is therefore necessary to define requirements that consider both the lunar environment and the operations to be performed, as shown in Table 8.

Table 8: Mobility System's requirements.

MOBILITY SYSTEM REQUIREMENTS LIST			
ID	Requirement name	Description	Ref.
	FUNCTIONAL RE	EQUIREMENTS	
LPR-FUN-M-010	Structural support	The mobility system shall	[15]
		support an habitat of 7000 kg	
LPR-FUN-M-020	Maximum speed	The rover shall reach a	
		maximum velocity of 30 km/h	
	Shock absorption	The mobility system shall	
LPR-FUN-M-030		ensure shock absorption	[3]
		capabilities	
LPR-FUN-M-040	Traction	The wheel shall transfer to the	
		ground enough traction to	[3]
		have the motion	

LPR-FUN-M-050	Low motion resistance	The motion resistances shall be as low as possible	[15]
LPR-FUN-M-060	Static stability	The mobility system shall maintain static stability on both flat terrain and inclined slopes	
	OPERATIONAL R	EQUIREMENTS	
LPR-OPS-M-010	Operative life	The mobility system shall ensure an operative life of 10 years	
LPR-OPS-M-020	Climbing steps	The rover shall climb steps up to 0.3 meters	
LPR-OPS-M-030	Climbing slopes	The rover shall climb slopes up to 20°	[4]
LPR-OPS-M-050	Backwards speed	The rover shall be capable of moving backwards at a maximum speed of $5 m/s$	
	DESIGN REQU	JIREMENTS	
LPR-DES-M-010	Flexible suspensions	The mobility system shall feature adaptable suspensions to adapt to lunar terrain and increase stability	
CONFIGURATION REQUIREMENTS			
LPR-CON-M-010	Driving wheels	The mobility system shall implement all-driving wheels	

The combined analysis of high-level requirements and specific mobility system requirements highlights the overall framework within which the pressurised rover must operate. The constraints represent a set of conditions that define the operational scope and design margins: autonomy and mission duration determine energy performance and power management strategies; environmental conditions determine the criteria for choosing materials and protection systems; mobility requirements, such as overcoming slopes, steps and complex terrain, guide the geometry of wheels, suspension and steering; the presence of a crew introduces safety and comfort constraints. In this context, the mission reference traverse becomes the operational formalisation of the boundary conditions set by the requirements.

3.3 Reference Traverse

The traverse scenario defines the boundary conditions derived from system requirements. A correlation can be defined between requirements, traverse scenario and preliminary design: the requirements drive the definition of the operational scenario, which provide the boundary conditions for dimensioning and performance assessment; the preliminary

design defines the validation point, ensuring consistency between requirements and technical implementation.

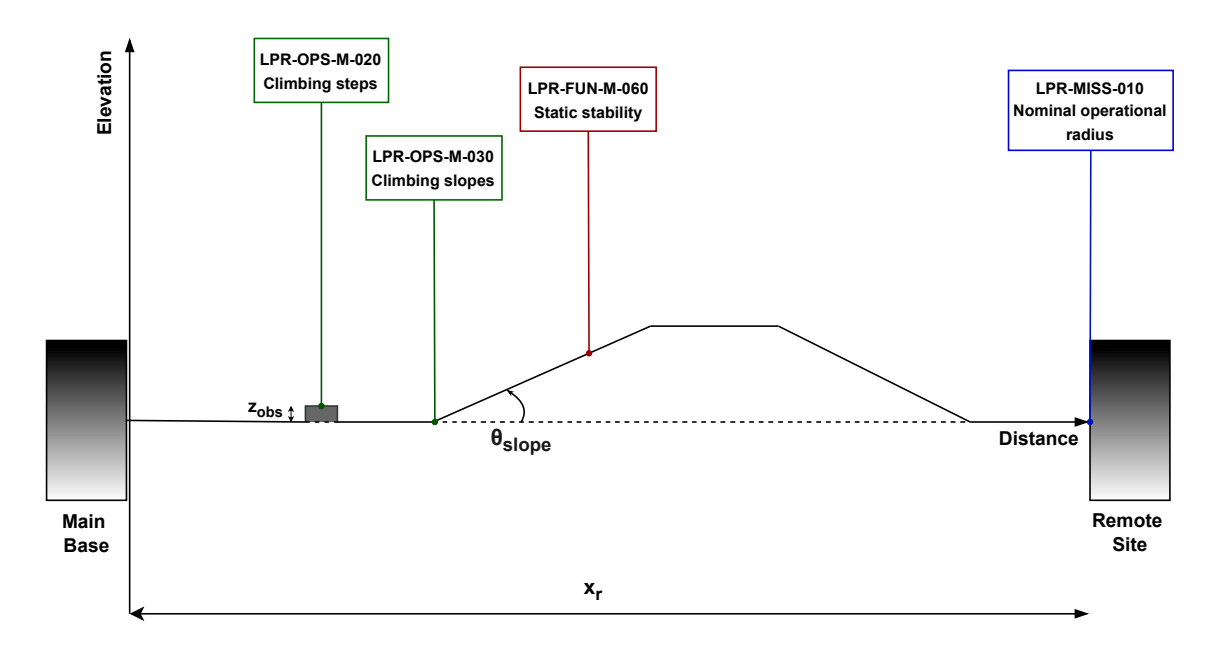


Figure 10: Reference traverse scenario.

The reference traverse in Figure 10 shows an operational scenario connecting the Main Base to the Remote Site. The representation is a simplified altimetric profile (altitude–distance), in which only the most stringent and decisive requirements for mobility have been selected. The objective is to identify the limit conditions that induce the most demanding loads for the locomotion system and have the most significant impact on rover's ability to perform the mission safely and effectively.

Four main requirements have been reported:

- Climbing steps (LPR-OPS-M-020) defines the maximum height of the obstacle (z_{obs}) that the rover must be able to overcome. This requirement affects the wheel geometry, the suspension stiffness and the torque available to climb the step without losing traction.
- Climbing slopes (LPR-OPS-M-030) establishes the maximum uphill and downhill slope (θ_{slope}) that can be approached. This limit condition has a direct relationship with traction performance, slip control, engine sizing and power requirements, and is representative of regolith ramps or crater rims that must be traversed under nominal operations.
- Static stability (LPR-FUN-M-060) is associated with the inclined section and ensures that the rover maintains a state of equilibrium without the risk of overturning. This requirement imposes constraints on the overall geometry of the vehicle, such as track width, wheelbase, centre of gravity position, and complete the slope requirement by shifting the focus from traction capability to system stability.
- Nominal operational radius (LPR-MISS-010) is represented by the total distance between the main base and the remote site (x_r) . This parameter defines the energy

budget allocated to mobility, establishes the autonomy limits of the power subsystem and introduces the mission-level constraint on the range of action, ensuring that the rover can perform its intended operational objectives with adequate safety margins.

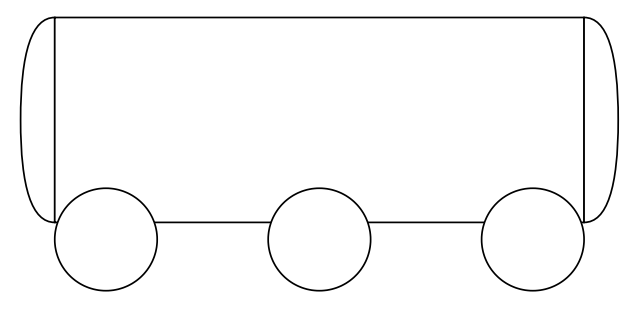
It must be noted that the locomotion system must meet a wider set of requirements, not directly stated in the reference traverse but contributing significantly to overall performance. These include operational requirements, such as minimum turning radius, which affects wheel kinematics and steering system configuration, and reverse motion capability, which is necessary to ensure safe manoeuvring. Equally important are functional requirements, such as maximum nominal speed or low rolling resistance, both closely dependent on wheels geometry and their interaction with the regolith.

4 Pressurized Rover Preliminary Design

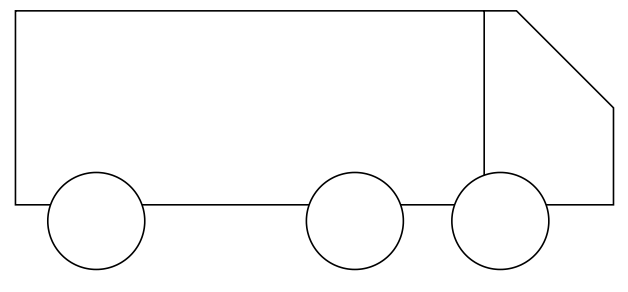
The preliminary design phase focuses on defining the overall geometry and maximum dimensions of the pressurised rover. These elements must ensure that the initial engineering solutions adopted simultaneously comply with mission constraints, such as the volume limits imposed by the launch vehicle fairing and the mass budget, and operational efficiency on the lunar surface.

4.1 Geometrical configurations

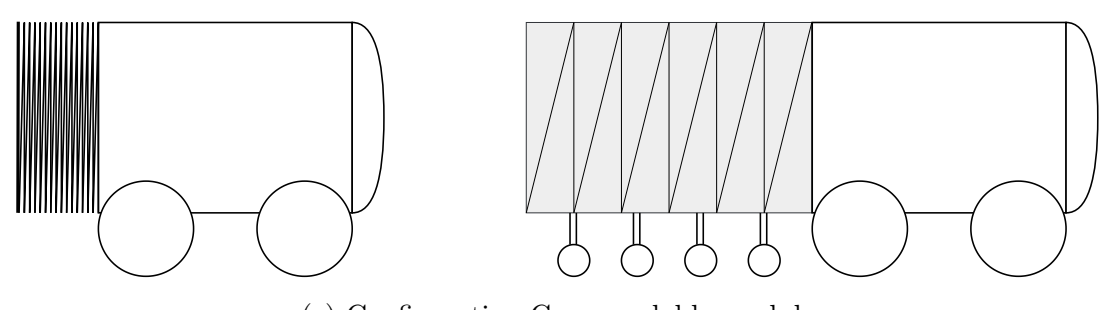
Three main configurations are analysed in this phase (Figure 11): cylindrical (Configuration A), Van-type (Toyota JAXA Lunar Cruiser [10]) (Configuration B), and compact drive with expandable rear module (Configuration C).



(a) Configuration A: cylindrical module



(b) Configuration B: Van-type



(c) Configuration C: expandable module

Figure 11: Rovers' geometry configurations.

4.1.1 Configuration trade-off

Each of the concept mentioned above is evaluated following a set of criteria:

- structural performance, including surface-to-volume ratio, pressure vessel efficiency and integration of openings;
- usability of internal volume, for habitability, crew operations and stowage;
- launch vehicle integration, considering packaging efficiency and accommodation in the fairing;
- operational conditions, such as stability, visibility and reliability on lunar surface;
- technological awareness and risk, due to a limited heritage and the complexity of the adopted mechanisms.

Each criterion is assigned a score from 1 to 5 (1 = poor performance, 5 = excellent performance). The results of this comparative assessment are shown in Table 9.

Configuration A: cylindrical module This configuration is the simplest and most efficient from a structural point of view, allowing the stresses generated by internal pressure to be distributed uniformly and minimising concentrated stresses. In addition, the surface area/volume ratio is favourable, with benefits in terms of structural mass and thermal management. These aspects make the cylindrical module an easily applicable and low-risk solution. The main limitation concerns the full use of internal volumes due to the curvature of the walls and the integration of hatches that require local reinforcement.

Configuration B: van-type This concept is characterised by the efficient use of its internal volume, facilitating the functional organisation of space. However, its structural efficiency is lower than that of the cylindrical configuration, as the internal pressure generates stresses that require increased stiffening and reinforcement, significantly increasing the mass and complexity of the vehicle. Furthermore, the surface area/volume ratio is less favourable, with an increase in the thermal loads to be managed.

Configuration C: expandable module This configuration features a compact motor with a deployable rear module. This solution minimises the maximum overall dimensions during launch and increases the internal volume once operational on the lunar surface. However, it presents several disadvantages due to its technological complexity: the deployment mechanisms, joints and sealing systems significantly increase operational risk, as these technological systems are not yet fully consolidated. Furthermore, the change in the centre of gravity between the stowed and expanded configurations can cause stability and dynamic control problems.

Table 9: Configuration trade-off.

Trade-off criterion	Config. A	Config. B	Config. C
Structural performance (S/V ratio, pressure efficiency, openings integration)	5	3	2
Internal volume usability	3	5	5
Integration with fairing	4	4	5
Operational conditions (stability, visibility, reliability)	4	4	3
Technological risk (complexity, TRL)	5	3	1
Total	21	19	16

4.1.2 Configuration chosen

The trade-off study shows that each of the configurations considered has specific advantages and limitations. The van-type configuration (B) provides the best overall efficiency in the use of internal volume and excellent habitability for extended missions, but with higher structural complexity and larger weights. The expandable configuration (C) is particularly favorable in terms of habitable volume and operational flexibility, but with very high levels of technological risk related to deployment and pressurization systems.

Given these considerations, the cylindrical configuration (A) is selected as the project baseline in this preliminary study. This focus is motivated by its simplicity of construction, high structural efficiency, and low technological risk, which facilitate its implementation in the early stages of design and ensure greater reliability in terms of performance and safety.

4.1.3 Fairing integration

A significant aspect in defining the rover's geometry concerns its integration with the launcher's fairing. The vehicle's dimensions must comply with the constraints imposed by the usable volume available, which is one of the main design drivers in the preliminary stages. In this case, the research is conducted with reference to the overall internal dimensions of the main commercial launch vehicles currently operating in the commercial launch sector. The cylindrical design, selected as the baseline, adapts to these geometric constraints thanks to its regular and compact cross-section, enabling optimal housing along the vertical axis of the fairing and reducing unused volumes. The parameters examined for this study concern the internal diameter, usable height, and maximum mass that can be transported into orbit. These values define the design margins within which

the rover configuration must fall. Since the launcher's performance strongly depends on the final orbit to be reached, the payload mass value is specified with reference to different orbital destinations: LEO, Geostationary Transfer Orbit (GTO) and Lunar Transfer Orbit (LTO).

Table 10 summarizes the main geometric and performance characteristics of the launch vehicles considered. As can be seen, the fairings of Falcon 9 and Ariane 6 have more stringent constraints, with internal diameters of around 5.2–5.4 meters and heights between 13 and 18 meters, requiring greater attention for configuration compactness. Starship and New Glenn offer significantly larger volumes, with diameters of up to 9 meters and heights of over 20 meters, allowing for wide margins for integration but with lower degrees of maturity and market availability compared to traditional launchers. Falcon Heavy represents an intermediate position, offering a compromise between capacity and operational integration. The final choice of launcher depends on the actual mass and dimensions of the rover, which will be described in the following sections.

	Ariane 6	Falcon 9	Falcon Heavy	Starship	New Glenn
$\overline{\text{Diameter } [m]}$	5.4	5.2	5.2	9.0	7.0
Height $[m]$	18.0	13.2	13.1	22.0	21.9
$m_{pay,LEO}$ [tons]	21.6	22.8	63.8	150	45
$m_{pay,GTO}$ [tons]	11.5	8.3	26.7	27	13.6
$m_{pay,LTO}$ [tons]	8.6	-	~21.0	-	7

Table 10: Launch vehicles comparison.

4.2 Preliminary Design and Sizing

The preliminary design aims to consolidate the geometric configuration of the rover in quantitative parameters, such as overall dimensions, mass balance, habitable volume, and subsystem distribution. These aspects must ensure both compliance with mission requirements and compatibility with the constraints imposed by the fairing of the launcher. At this stage, the sizing process is guided by analytical formulations and the application of engineering margins, in order to provide a consistent framework for subsequent analyses at the subsystem level.

4.2.1 Overall dimensions

The selected geometry allows the external volume of the pressurized rover to be estimated as a combination of a cylinder and two semi-spherical bulkheads. The overall dimensions of the pressurized module, set to $D_{LPR} = 3.07 \ m$ and $L_{LPR} = 7.10 \ m$, are determined

by considering a combination of external constraints and internal requirements. From a geometric point of view, the diameter of the cylindrical section and the overall length were chosen respecting the requirements related to the minimum habitable volume necessary to ensure adequate living conditions for the crew and, at the same time, considering the limits imposed by the launcher fairing.

As mentioned in section 4.1.2, the pressurized module is modeled as a cylinder of length L_{cyl} and radius R, connected at its extremes to two semi-spherical end-caps with an axial depth h. Figure 12 shows the main geometric parameters of the pressurized module in a 2D side view, highlighting the main characteristics.

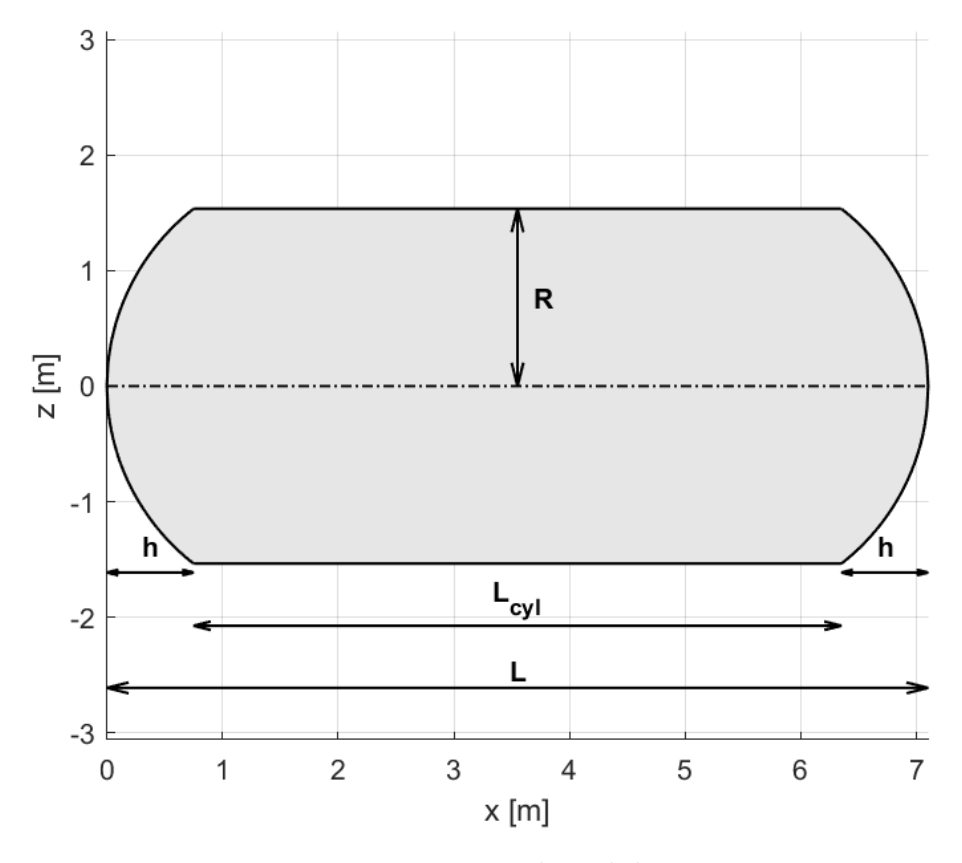


Figure 12: Pressurized module size.

The total external volume of the habitat can be expressed as

$$V_{tot} = V_{cul} + 2V_{sph} \tag{1}$$

where

$$V_{cyl} = \pi R^2 L_{cyl} \tag{2}$$

$$V_{sph} = \frac{\pi h^2 (3R_s - h)}{3} \tag{3}$$

These two terms respectively refer to the cylindrical volume and to the volume of the two semi-spherical end-caps. In Eq. (3), $R_s = \frac{R^2 + h^2}{2h}$ represents the radius of the generating sphere that defines the end-cap geometry.

To determine the internal usable volume of the module, it is necessary to define the thickness of the pressure vessel. The internal pressure values adopted for habitable space modules generally vary between 34.5 kPa and 101 kPa; a typical design choice of around 69 kPa, as reported in [24], ensures a compromise between comfort, physiological safety, and reduction of structural mass.

In accordance with this requirement, the theoretical thickness calculated for a cylindrical shell with radius $R=1.53\ m$ would be in the order of 1–3 mm depending on the material used. However, to ensure robustness under other loads (launch, interfaces, openings), a uniform thickness of $t=5\ mm$ is adopted for the pressurized shell in the preliminary phase. This choice represents a conservative value that will be subsequently refined through FEM analysis and the definition of local reinforcements.

Assuming the uniform thickness for the pressurized vessel, the internal geometry and its available volume can be estimated. As a first approximation, the internal radius is

$$R_i = R - t \tag{4}$$

while the inner radius of the spherical shell can be calculated as

$$R_{s,i} = \frac{R_i^2 + h_i^2}{2h_i} \tag{5}$$

where $h_i \approx h - t$ represents the axial depth of the internal semi-spherical bulkhead.

The total internal volume can be estimated as

$$V_{int} = V_{cyl,i} + 2V_{sph,i} = \pi R_i^2 L_{cyl,i} + 2\frac{\pi h_i^2 (3R_{s,i} - h_i)}{3}$$
(6)

Once the structural thickness of the shell is defined and the internal volume of the module calculated, the available space for the crew during nominal operations, referred to as the Net Habitable Volume (NHV), can be determined. The net volume is obtained by subtracting from the internal volume all the volumes related to the subsystems and internal infrastructure, including the floor, ECLSS, avionics, tanks, as well as furnishings, workstations, and storage elements.

Since a detailed layout is not yet available, volumetric utilization coefficients η_{hab} , typically between 0.60 and 0.80, are adopted to conservatively estimate the ratio between net volume and internal volume

$$V_{net} \approx \eta_{hab} V_{int} \tag{7}$$

An additional evaluation metric is introduced in [25] and concerns the volume per person (V_{pp}) . For short-duration missions (days to weeks), the minimum net volume requirement per astronaut is typically in the range of 2–5 m^3 per person, while for long-duration missions (several months to years), more comfortable values are between 25 and 40 m^3 per person. The volume per person can be defined as

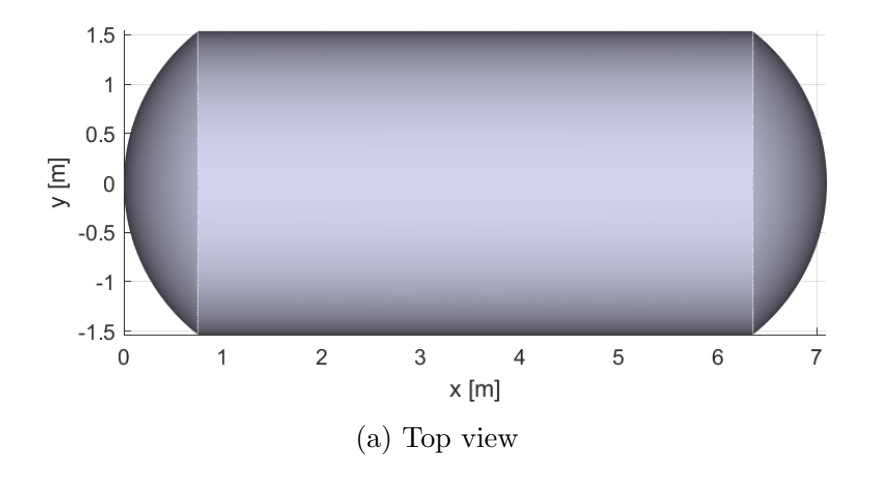
$$V_{pp} = \frac{V_{net}}{N_{crew}} \tag{8}$$

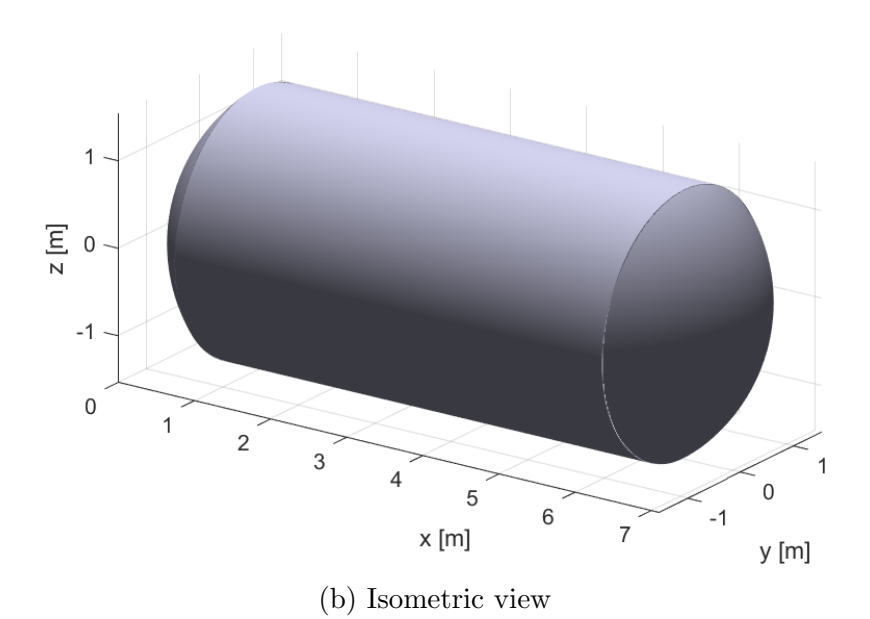
Table 11 summarizes the geometric parameters of the pressurized module. Considering the reference mission duration defined in the mission requirements, the net habitable volume per person medium-duration missions is adequate and consistent with the specifications outlined in [25].

Table 11: Summary of overall dimensions for the pressurized module.

Parameter	Symbol	Value	Unit
Cylindrical volume	V_{cyl}	41.45	m^3
Semi-spherical bulkhead volume	V_{sph}	2.99	m^3
Total external volume	V_{tot}	47.45	m^3
Vessel thickness	\mathbf{t}	0.005	m
Internal volume	V_{int}	47.09	m^3
Net volume	V_{net}	35.32	m^3
Volume per person	V_{pp}	17.66	m^3

The 3D reconstruction of the pressurized module is shown in Figure 13. These representations are intended to provide a more immediate visualization of the spatial configuration of the habitable volume, offering an initial tool for the qualitative evaluation of the integration of subsystems, the distribution of useful volumes, and the internal organization of spaces intended for the crew.





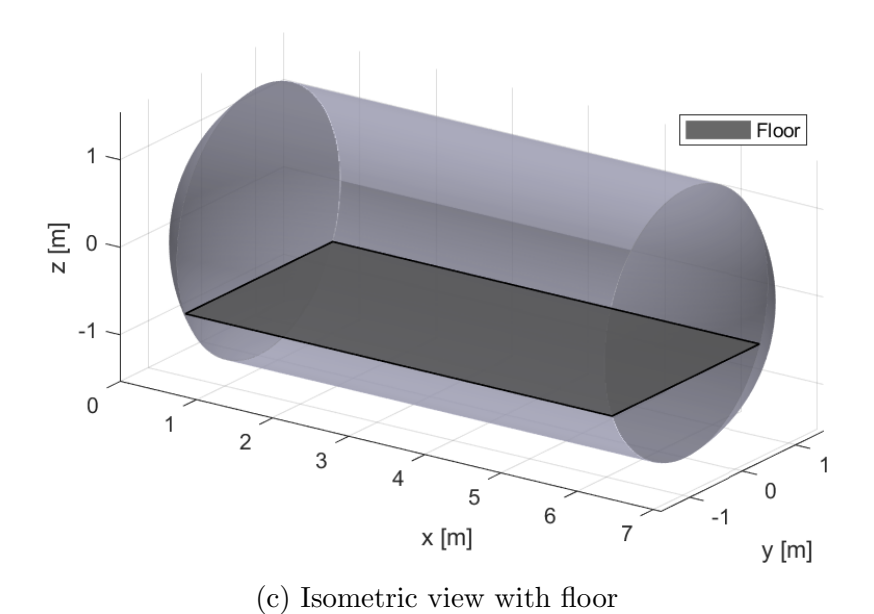


Figure 13: Pressurized module 3D view.

In addition to the volume of the pressurized module, a basic assessment of the rover's overall dimensions must also take into account the mobility system, including wheels, suspension, and steering mechanisms. In the preliminary phase the most established approach in the geometric packaging phases is to determine an external envelope (or bounding box) that encloses the entire vehicle, integrating the pressurized body with the geometric margins deriving from the position of the axles and the lateral and longitudinal clearance requirements. In this study, the envelope is calculated based on the geometric parameters available in the preliminary design:

$$L_f, L_r, L_{bf}, L_{br}, T, h_{cl}, h_{top}$$

where L_f and L_r represent the center of gravity—axle distances, L_{bf} and L_{br} the axle—bumper distances, T the transverse track, h_{cl} the ground clearance of the lowest point of the module and h_{top} a height margin for upper appendages, such as antennas and sensors. Due to the lack of a detailed definition of the wheels, suspension, and steering mechanisms, the vehicle envelope is determined considering the static configuration of the rover when the pressurized body is in equilibrium with respect to the axes and the ground. The equations that define the vehicle envelope can be expressed as

$$x_{env} = L_{bf} + L_f + L_r + L_{br} \tag{9}$$

$$y_{env} = T + 2b_{wheel} \tag{10}$$

$$z_{env} = D_{LPR} + h_{cl} + h_{top} \tag{11}$$

where the width of the wheel b_{wheel} is assumed to be the typical maximum width of pressurized rover concepts, equal to 0.5 m. The main parameters related to the definition of the overall envelope of the pressurized rover are shown in Table 12.

Table 12: Summary of envelope dimensions.

Parameter	Symbol	Value	Unit
Front CG-axle distance	L_f	3.10	m
Rear CG–axle distance	L_r	3.10	m
Front axle–bumper distance	L_{bf}	0.45	m
Rear axle-bumper distance	L_{br}	0.45	m
Overall length	$x_{ m env}$	7.10	\mathbf{m}
Transverse track	T_c	3.10	m
Wheel width (max)	b_w	0.50	\mathbf{m}
Overall width	$y_{ m env}$	4.10	\mathbf{m}
Ground clearance	h_{cl}	0.60	m
Module diameter	D_{LPR}	3.07	\mathbf{m}
Top margin (antennas/sensors)	h_{top}	0.50	m
Overall height	$z_{ m env}$	4.17	m

The figure shows the 3D model of the envelope, which encloses the entire vehicle by integrating the pressurized module with the mobility system. This representation allows

for an initial assessment of the rover's overall proportions and the verification of its compatibility with the fairing constraints.

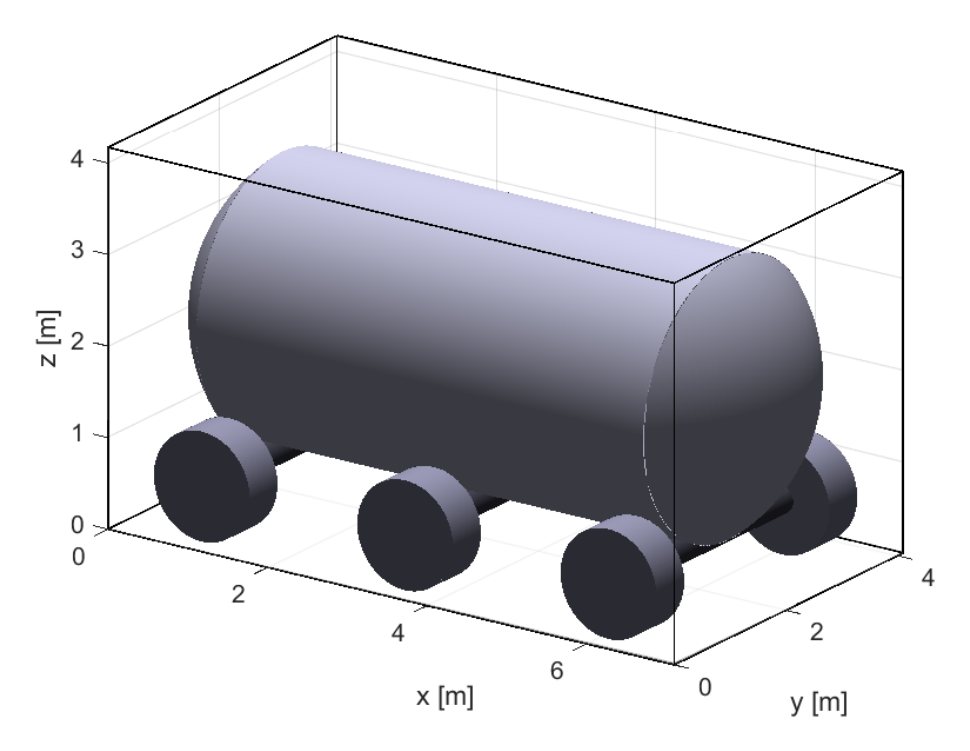


Figure 14: Envelope of the pressurized rover.

4.3 Subsystems

The overall architecture of a pressurized lunar rover is defined by the integration of its subsystems. Each subsystem must meet specific functional requirements and introduce additional mass, volume, and power constraints. The pressurized rover combines an integrated habitat—vehicle system: as a habitat, it must provide life support, protection, and comfort for the crew (through ECLSS, thermal control, communications, radiation shielding); as a vehicle, it must ensure mobility, stability, power, and autonomous navigation capabilities on rough terrain.

4.3.1 Structure

The Structure is responsible for the structural support of the living module, the transmission of loads from the wheels and suspension, and the integration of mobile mechanisms. During the design phase, sufficient stiffness must be ensured to withstand dynamic loads, such as acceleration during launch and vibrations, as well as static loads during internal pressurization, and impacts on the lunar surface. The choice of materials (light alloys, composites, sandwich structures) must be a balance between weight and protection from micrometeorites and radiation.

4.3.2 Mobility

The mobility enables the rover to move effectively on uneven lunar terrain. It includes non-pneumatic wheels (metal mesh, flexible composite materials) designed to withstand regolith abrasion and thermal stress, independent suspension or modified rocker-bogie systems, front/rear steering, and electric transmission. The design takes into account the mass of the rover, the load per wheel, the power required to move on slopes and regolith, and the durability for distances of hundreds of kilometers. Typical expected performance includes operating speed, obstacle clearance, long range, and robustness.

4.3.3 TCS

The Thermal Control System (TCS) is responsible for regulating temperatures in the various subsystems and the habitat, ensuring that operating temperatures do not exceed the limits for the crew, batteries, electronics, and mechanical components. Given the wide temperature range on the Moon, the TCS must combine passive capabilities (insulation, MLI, reflective coatings) and active capabilities (heat pipes, heat sinks, electric heaters).

4.3.4 EPS

The Electrical Power System (EPS) is responsible for generating, storing, and distributing energy to all subsystems. Common selections include high-efficiency solar panels or hybrid/fuel cell systems. Storage is typically provided by Li-ion batteries connected to a Battery Management System (BMS) that controls charging/discharging and cell balancing. Energy distribution requires redundant Power Distribution Unit (PDU), and the most important systems, such as ECLSS and avionics, have dedicated lines. The system must also comply with power margins for transient loads, predict losses (due to resistance and cabling), and manage coupling with the TCS to dissipate the heat generated by the batteries.

4.3.5 GNC

The Guidance, Navigation and Control (GNC) is responsible for calculating the rover's position, velocity, and attitude and regulating its motion based on feedback. It includes sensors such as Inertial Measurement Unit (IMU), wheel odometers, stereo cameras and navigation algorithms. Actuators respond to GNC commands to maintain desired trajectories and stability.

4.3.6 ECLSS

The ECLSS includes the generation, regulation, and recirculation of the atmosphere (oxygen, nitrogen, CO_2 control, humidity), water treatment and recycling (urine, condensation, storage), and controlled waste disposal. The sizing of ECLSS is based on

human metabolic load (oxygen required, CO_2 production, heat to be dissipated), as well as the desired autonomy time and reserve factor. The system must be robust and redundant, and capable of interfacing with the Command and Data Handling (CDH), EPS, laboratory, and habitat.

4.3.7 CDH

The CDH subsystem handles uplink commands, real-time subsystems control, and internal data management. It serves as interface among payload, avionics, ECLSS, GNC, and Communication System (COMMS): it receives data from sensors, manages sequences, and reacts to failures. The CDH includes one or more redundant embedded computers, mass storage, high-speed data buses, real-time software, and analog/digital I/O modules. It must be designed to tolerate interference and radiation while ensuring reliability and reconfigurability.

4.3.8 COMMS

The COMMS manages the communications between the rover and the external environment: it includes antennas (omnidirectional, directional), transmitters, receivers, amplifiers (Low Noise Amplifier, High Power Amplifier), filters, transponders, modulators, and interfaces with the on-board electronics. The COMMS must meet requirements for link budget, data rate, power margins, and compatibility with orbital networks or ground infrastructure. It must also support modes for EVA (local communications), telemetry, uplink and downlink scientific and navigation commands.

4.3.9 Summary of Subsystems

To conclude the description of the individual subsystems, Table 13 provides a summary of their main functions and critical interfaces with other elements of the vehicle. This summary provides a reference tool for the preliminary design phase, highlighting the interdependencies between subsystems that influence the overall configuration of the rover.

Table 13: Summary of subsystems.

Subsystem	Functions	Critical interfaces
Structure	Ensuring mechanical integrity, support habitats and mobility, withstand pressurization	Mobility (load transmission), Habitat (pressurized sealing), EVA support (doors/suitports)
Mobility	Enabling locomotion on regolith	Structures, EPS (motors), GNC (steering/speed control)

TCS	Maintaining operating temperatures for crew and avionics	EPS (batteries), Habitat (comfort), Structure (insulation), External radiators
EPS	Energy generation, storage, and distribution	TCS (battery cooling), CDH (power bus), Mobility (motors)
GNC	Determination and control of position, speed, and attitude	Mobility (wheel/steering actuators), CDH (algorithms), EPS (sensor power supply)
ECLSS	Monitoring the atmosphere, water, waste	Habitat (air), EPS (pumps/fans), TCS (heat exchangers), CDH (monitoring)
CDH	Command management, telemetry, and internal data	COMMS (uplink/downlink), GNC (sensor fusion), ECLSS (telemetry)
COMMS	Internal and external communications	CDH (data packages), Structure (antennas), EPS (amplifiers)

The total mass of the pressurized lunar rover is thus preliminarily set to $M_{tot} = 7000 \ kg$, consistent with reference designs such as NASA's SEV [9] and JAXA's Lunar Cruiser [10]. This value includes the habitable module, mobility subsystems, power, and life-support equipment, and serves as the baseline for subsequent study of the suspension and wheel systems.

5 Locomotion System Design

The development of a locomotion system for a lunar rover requires the adoption of a rigorous and systematic methodology capable of combining mission requirements with terramechanical modeling and subsequent phases of overall system evaluation.

The adopted approach is outlined in Figure 15. Starting from the definition of the mission and high-level requirements, a preliminary performance assessment is conducted using terramechanical models, followed by the definition of possible locomotion architectures. After selecting the reference architecture and conducting an initial analysis of the system, the architecture is consolidated and validated. The locomotion system is dimensioned, complemented by a second-level analyses, until the final verification of compliance with the project requirements.

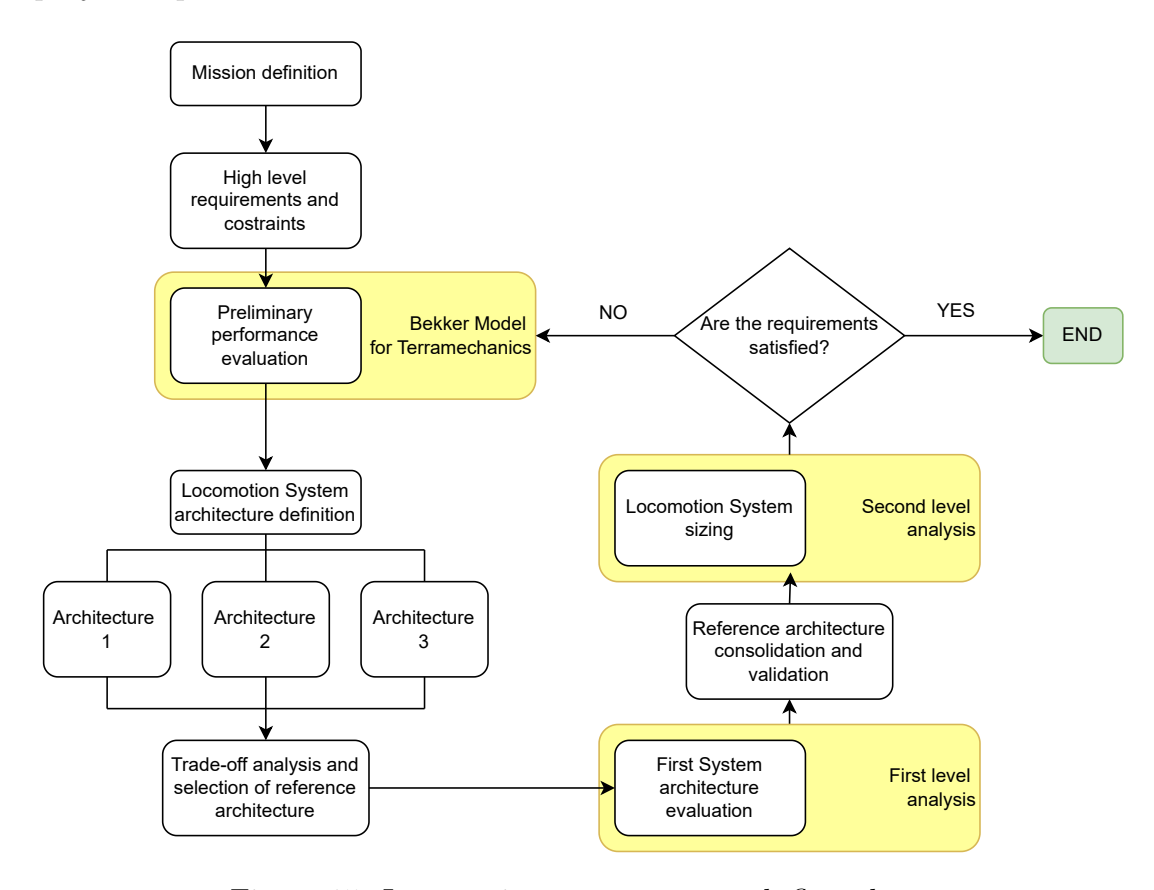


Figure 15: Locomotion system approach flow-chart.

5.1 Terramechanical Model

For the study of the mechanical response of the terrain under the influence of external forces, such as vehicle load and traction, Bekker's Derived Terramechanics Model (BDTM) is implemented. This represents an established analytical method used to predict the off-road mobility of vehicles, incorporating the Bekker's equations [26].

A comprehensive study of the lunar soil is essential as its mechanical behavior varies considerably depending on environmental and material factors: various properties, such as soil composition, density and moisture can influence the soil's response to stress and deformation. Besides, these variations can affect fundamental characteristics such as bearing capacity, shear force and, more generally, vehicle dynamics.

Through a parallel study of ground properties and vehicle performance, the Bekker's model provides a fundamental basis for the design and evaluation of off-road vehicles, especially in applications where terrain conditions are highly variable, such as extrater-restrial exploration sites.

To clearly describe the procedure employed in the terramechanical approach, the diagram shown in Figure 16 has been developed, illustrating the main steps of the model.

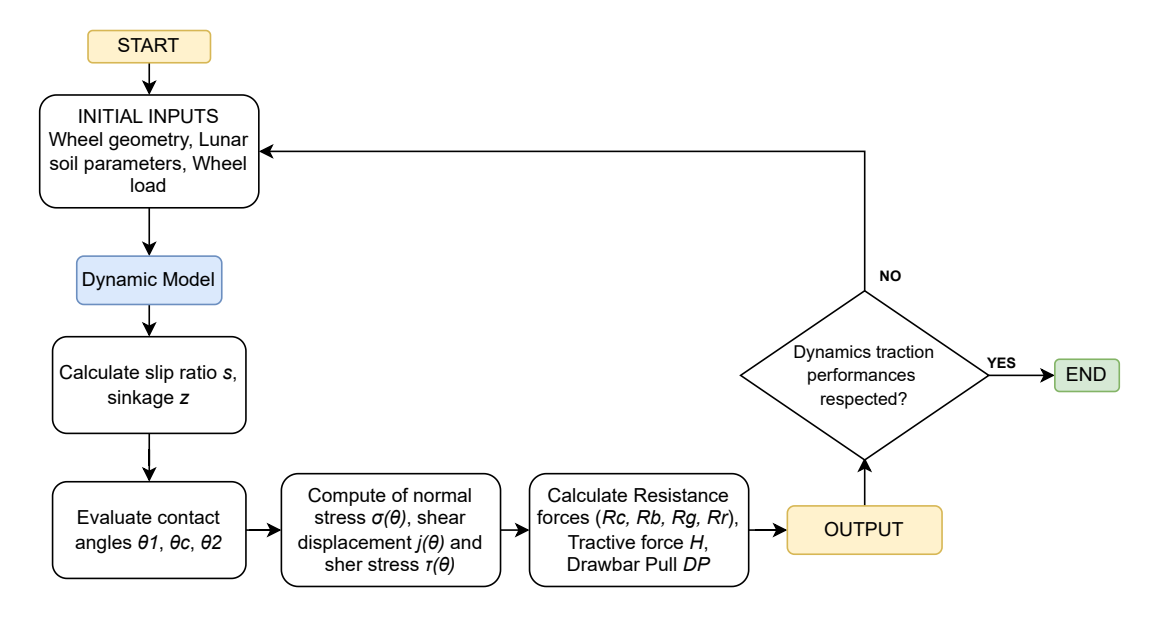


Figure 16: Diagram of the implemented terramechanical model.

5.1.1 Lunar Soil

Lunar regolith consists of a mixture of five types of particles: crystal rock fragments, mineral grains, breccias, agglutinates and glasses. There are variable amounts of these materials throughout the lunar environment, based on the local rock composition and the geological processes that acted on them. Additionally, as concerns the particle shape, it can be highly variable, particularly with respect to elongation (the ratio of the major to intermediate axes). As a result, the material properties are anisotropic, which affects the compression and shear strength of the lunar soil. Experimentally, the physical properties of lunar soil have been studied in a number of ways, either through in-situ measurement, laboratory analysis on returned samples, or observation from orbiting the Moon [4].

The factors that most influence wheel-soil interaction are primarily related to the soil's geotechnical properties, such as density, and mechanical properties, such as compressibility and shear strength. These properties determine the soil's engineering parameters, including bearing capacity, slope stability and trafficability.

A description of each of these factors, which are useful for the study of terramechanics, is given below.

Density ρ The mass of the material contained within a given volume, usually expressed in g/cm^3 . This parameter has been analysed in detail to determine its dependence on the depth at which measurements are taken, obtaining the following empirical formulation:

$$\rho = 1.92 \left(\frac{z + 12.2}{z + 18} \right) \tag{12}$$

In Table 14 a summary of typical average values of lunar soil density as a function of depth is shown [27].

Table 14: Average density as a function of depth range.

Depth Range [cm]	Typical Average Density Values ρ $[g/cm^3]$
0 - 15	1.50 ± 0.05
0 - 30	1.58 ± 0.05
30 - 60	1.74 ± 0.05
0 - 60	1.66 ± 0.05

Compressibility The densification of the material when stress is applied to the soil. The entity of compression depends on the initial conditions: with low stress or low density the result is particles' slippage, while for higher stresses or high densities deformation phenomena of the particles occur at the contact points. This phenomenon becomes relevant when the vehicle's wheel exerts a force on the ground below, which tends to compact.

The degree of compression can be evaluated using the Compression Index C_c , defined as

$$C_c = -\frac{\Delta e}{\Delta \log(\sigma_v)} \tag{13}$$

where $\Delta e = V_v/V_s$ is the ratio of the volume of voids between particles and the solid volume of soil and $\Delta \log(\sigma_v)$ is the variation of applied vertical stress on logarithmic scale. Several experiments were conducted on samples from the Apollo 12 mission, obtaining an average compression value for lunar soil equal to Cc = 0.3 [4].

Shear Strength τ The maximum shear stress the soil can sustain without failure. The soil portion reaches its failure point when the shear stress satisfies the Mohr–Coulomb equation

$$\tau = c + \sigma \tan(\phi) \tag{14}$$

where τ is the shear strength of the material, c is the cohesion of the material, σ is the normal stress, and ϕ is the angle of internal shearing resistance of the material, or friction angle [26].

Based on data collected during Apollo missions, the following results are reported for cohesion and friction angle as a function of depth

Table 15: Cohesion and friction angle values as a function of depth range.

Depth Range [cm]	Cohesion Values $[kPa]$	Friction Angle Values $[deg]$
0 - 15	0.44 - 0.62	41 - 43
0 - 30	0.74 - 1.1	44 - 47
30 - 60	2.4 - 3.8	52 - 55
0 - 60	1.3 - 1.9	48 - 51

Bearing Capacity The ability of the soil to support an applied load. At low applied loads, the soil below the surface is in static equilibrium, and it experiences elastic deformation and compression. As the load further intensifies, the soil enters a state of plastic deformation and the sinkage increases significantly, as shown by the Z_c curve in Figure 17.

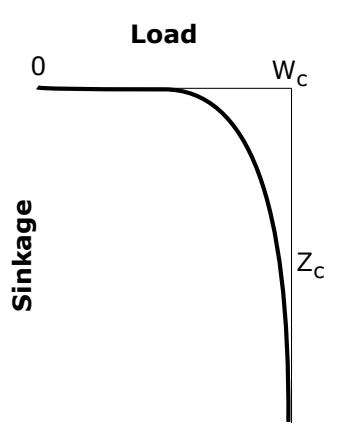


Figure 17: Soil deformation as a function of the load.

 W_c represents the Terzaghi Bearing Capacity, which is the vertical load at which the soil experiences plastic deformation and sinkage (Z_c) . It is defined as follows:

$$W_c = 2\gamma lb^2 N_\gamma + 2lb\sigma N_q + \frac{4}{3}lbcN_c \tag{15}$$

where c is the soil cohesion, γ is the specific gravity, b is the wheel's width, l is the length of contact of the wheel. N_{γ} , N_{q} and N_{c} are the bearing capacity factors and they are dependent on the friction angle ϕ (Figure 18). These factors will be further analyzed in the next section.

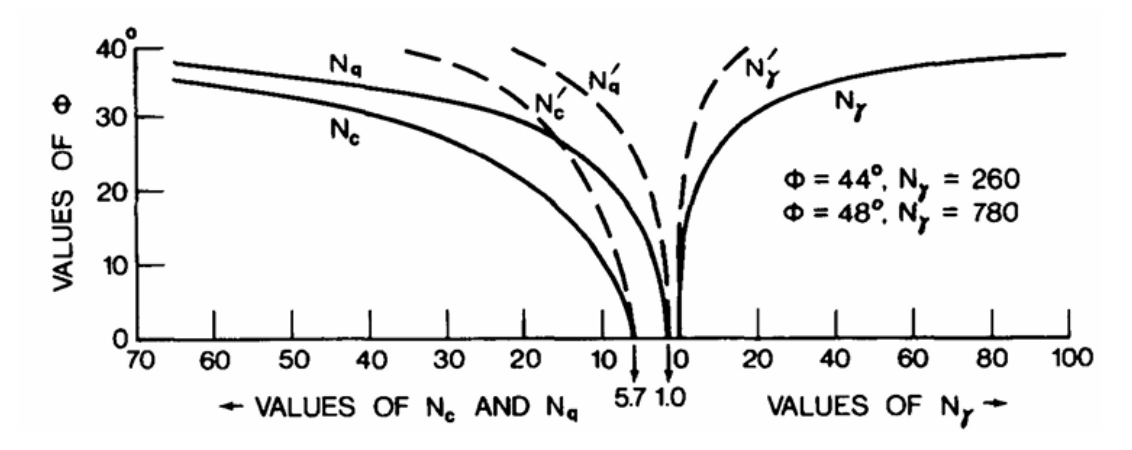


Figure 18: Variation of the Terzaghi Bearing Capacity factors with the angle ϕ [26].

Slope stability The ability of the soil to stand without support. To avoid a slip failure of the lunar soil a safety factor is defined [4]

$$S.F. = N \frac{\rho g_{moon} h}{c} \tag{16}$$

where ρ is the density of soil, c is the soil cohesion, g_{moon} is the gravity on the Moon, h is the height of the slope and N is the stability number, which is a function of the friction angle and the slope angle.

Despite the lack of data, several hypotheses have been formulated regarding the limited stability of the soil, including slow soil movements (soil creep), soil outgassing during shear that creates fluidized conditions and pseudofluidization due to bouncing particles. However, the stability of the soil on slope condition remains unclear and requires further investigation.

Trafficability The capacity of a soil to support a vehicle and to provide sufficient traction for movement. In order to comply with traffic conditions, it is necessary to choose configurations that maximise soil thrust and minimise resistance.

5.1.2 Wheel-soil interaction

In the representation of the wheel-ground contact, the model assumes the contact area to consist of three distinct and consecutive sections: the front section of the wheel, the deflected (flat) section of the wheel and the rear section of the wheel. The front and rear sections are modelled as curved surfaces, while the deflected centre section is treated as a flat area resulting from the flexibility of the wheel. The distribution of stresses within each section is formulated as a function of multiple influencing factors, including the mechanical parameters of the terrain (such as cohesion and internal friction) and the operating parameters of the wheel (such as slip ratio and forward speed). In developing this model, the following assumptions are considered:

• the deflected area BC is horizontally flat and the normal stress beneath the flat section is uniformly distributed;

- the contact patch of the sections AB and CD are circular arc;
- the normal stress in the wheel width direction is uniformly distributed.

In this model, the wheel-soil interaction is initially studied by considering the static sinking of the wheel and its deflection due to the wheel load, followed by the calculation of the stresses to which the wheel is subjected and finally the forces and torques are obtained.

5.1.3 Static model

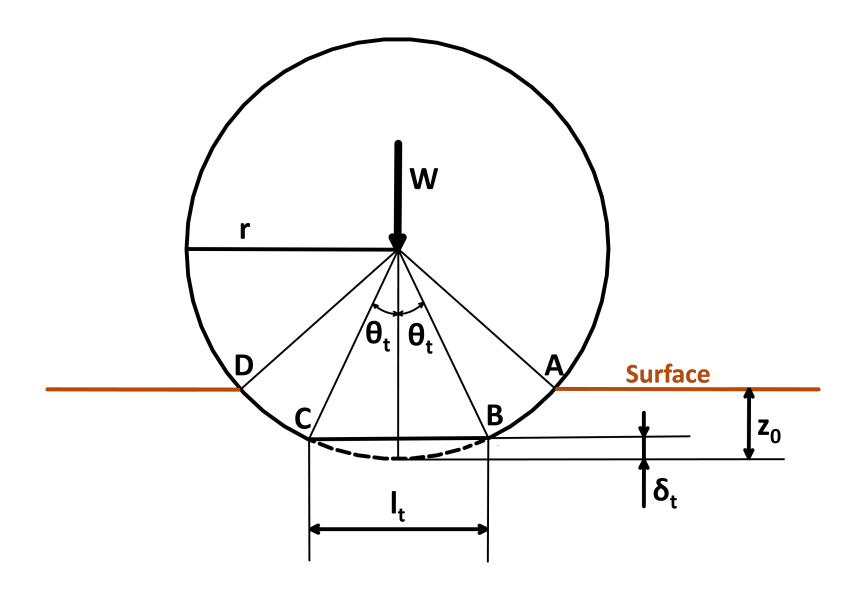


Figure 19: Representation of the wheel in static conditions.

To determine static conditions, it is assumed that the wheel is not rotating and it is subjected to a certain deflection δ_t and a static sinkage z_0 . Under these conditions, a vertical reaction force F_{z0} is generated, which must balance the external wheel load W applied to the system. F_{z0} is derived from the contribution of two forces

$$F_{z0} = F_w + 2F_s \tag{17}$$

where F_w is the force generated at the flat section BC and $2F_s$ is the force at the front and rear sections AB and CD.

The force at section BC can be calculated as follows

$$F_w = P_w b l_t \tag{18}$$

where P_w represents the wheel pressure due to its structural stiffness, b is the wheel width and l_t is the horizontal length of the flat section.

The force F_s can be expressed as a function of wheel diameter D and width b, cohesive modulus k_c , frictional modulus k_{ϕ} , static sinkage z_0 , sinkage exponent n and wheel deflection δ_t

$$F_s = \left[b \left(\frac{k_c}{l_t} \right) + k_\phi \sqrt{D} (z_0 + \delta_t)^{n-1} \right] \cdot \frac{(3-n)[(z_0 + \delta_t)^{3/2} - \delta_t^{3/2}] - 3z_0 \sqrt{\delta_t}}{3}$$
(19)

while the length of the flat section and the static sinkage can be respectively calculated as

$$l_t = 2\sqrt{D\delta_t - \delta_t^2} \tag{20}$$

$$z_0 = \begin{cases} \left(\frac{P_w}{k_c/l_t + k_\phi}\right)^{1/n} & \text{if } l_t < b\\ \left(\frac{P_w}{k_c/b + k_\phi}\right)^{1/n} & \text{if } l_t \ge b \end{cases}$$

$$(21)$$

An appropriate value of the wheel deflection δ_t can be derived by implementing an iterative approach, such as the bisection method: an initial value of the deflection is estimated in order to calculate the values of l_t , z_0 and the reaction force F_{z0} using the force equilibrium equation. The value of δ_t is determined when F_{z0} is equal to W.

5.1.4 Dynamic model

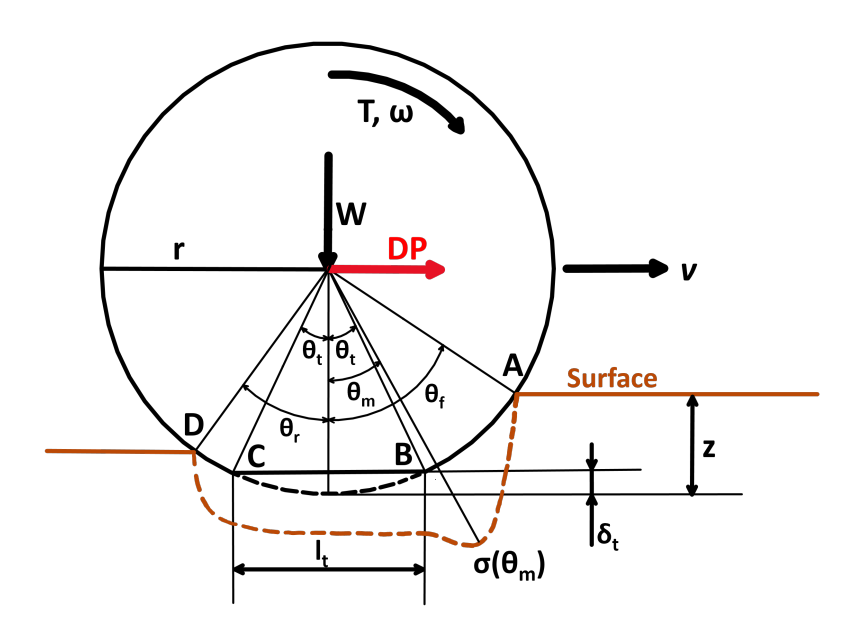


Figure 20: Representation of the wheel in dynamic conditions.

Once the value of the δ_t deflection is obtained, it is possible to proceed with the calculation of the stresses and forces. In relation to the normal stress distribution, the following calculation method is employed respectively for front, flat and rear sections, contingent on the wheel-soil contact angle, denoted by θ :

$$\sigma(\theta) = \begin{cases} \sigma_f = \sigma_m(\cos\theta - \cos\theta_f)^n \\ \sigma_t = \begin{cases} \left(\frac{k_c}{l_t} + k_\phi\right)(z - \delta_t)^n & \text{if } l_t < b \\ \left(\frac{k_c}{b} + k_\phi\right)(z - \delta_t)^n & \text{if } l_t \ge b \end{cases} \\ \sigma_r = \sigma_m \left(\frac{\cos\theta_f - (\theta - \theta_r)(\theta_f - \theta_m)}{\theta_m - \theta_r} - \cos\theta_f\right)^n \end{cases}$$
(22)

where

$$\sigma_m = r^n (k_c/b + k_\phi) \tag{23}$$

$$\theta_f = \arccos\left(1 - z/r\right) \tag{24}$$

$$\theta_r = \arccos\left(1 - \lambda z/r\right) \tag{25}$$

with λ is a parameter representing soil rebound-ness due to elasticity.

The stress σ and angle θ to be considered for each section is given in the Table 16.

Table 16: Equation for normal stress at each contact section.

$$\frac{\sigma(\theta) | \text{ if } \theta_m > \theta_t | \text{ if } \theta_m \leq \theta_t}{\sigma_f | \theta_m \leq \theta \leq \theta_f | \theta_t \leq \theta \leq \theta_f}$$

$$\frac{\sigma_t | \theta_m \leq \theta \leq \theta_f | \theta_t \leq \theta \leq \theta_f}{\sigma_t | \theta_t \leq \theta \leq \theta_t | \theta_t \leq \theta \leq \theta_t}$$

$$\frac{\sigma_r | \theta_t \leq \theta \leq \theta_m}{\theta_r \leq \theta \leq \theta \leq \theta_t} | \theta_r \leq \theta \leq \theta_t$$

The angle θ_m , at which the normal stress reaches its maximum, is modelled as

$$\theta_m = (a_0 + a_1 s)\theta_f \tag{26}$$

The two empirical parameters a_0 and a_1 depend on wheel-soil interaction, s is the slip ratio, as a function of the circumferential velocity $r\omega$ and longitudinal velocity v of the wheel, defined as

$$s = \begin{cases} \frac{r\omega - v}{r\omega} & for \ driving \ condition \\ \frac{r\omega - v}{v} & for \ braking \ condition \end{cases}$$
 (27)

As a function of slip ratio and contact angle, the soil deformation can be calculated as

$$j(\theta) = \begin{cases} r[\theta_f - \theta - (1 - s)(\sin \theta_f - \sin \theta)] & \text{for front and rear section} \\ j(\theta_t) + s(r\sin \theta_t - (r - \delta_t)\tan \theta) & \text{for flat section} \end{cases}$$
(28)

Once the soil deformation is determined, the shear stress $\tau(\theta)$ is obtained

$$\tau(\theta) = [c + \sigma(\theta) \tan \phi][1 - e^{-j(\theta)/k}] \tag{29}$$

The vertical force F_z is the result of the integration of the normal and shear stresses at each section of wheel contact patch

$$F_z = rb \int_{\theta_t}^{\theta_f} [\tau(\theta)\sin\theta + \sigma(\theta)\cos\theta]d\theta + \sigma_t bl_t + rb \int_{\theta_r}^{-\theta_t} [\tau(\theta)\sin\theta + \sigma(\theta)\cos\theta]d\theta$$
 (30)

Driving Resistances Based on reasonable values for the wheel diameter and width, in accordance with the weight and speed requirements, the driving resistances are analysed as a function of a diameter range between 0.8 and 1.4 metres and a width range between 0.3 and 0.9 m.

Four main resistances are considered: compaction, bulldozing, rolling and gravitational.

• Compaction Resistance: on soft lunar soil, the wheels of a lunar rover are subjected to several forms of resistance that reduce its ability to move effectively on the surface. When a wheel passes over lunar soil, the ground underneath is compacted due to the pressure caused by the wheel itself. This compaction process creates a form of resistance known as compaction resistance. Among the different types of resistance encountered during driving, compaction resistance is considered the main component of driving resistance, especially when the vehicle is driving through flat, soft terrain such as that found on the Moon and it can be calculated as

$$R_c = rb \int_{\theta_*}^{\theta_f} \sigma_f(\theta) \sin \theta d\theta - rb \int_{\theta_*}^{\theta_r} \sigma_r(\theta) \sin \theta d\theta$$
 (31)

• Bulldozing Resistance: during the motion of the rover, a portion of soil tends to be pushed and accumulate in front of the wheels, generating a resistance called bulldozing resistance. This resistance is also a significant component of the total resisting force and therefore needs to be accurately assessed as it depends on many factors, including soil properties, wheel design and sinkage z. The bulldozing resistance can be formulated as

$$R_b = \frac{b\sin(\alpha + \phi)}{2\sin\alpha\cos\phi} \left(2zcK_c + \gamma z^2K_\gamma\right) + \frac{l_0^3\gamma}{3} \left(\frac{\pi}{2} - \phi\right) + cl_0^2 \left[1 + \tan\left(\frac{\pi}{4} + \frac{\phi}{2}\right)\right]$$
(32)

Bulldozing is influenced by several factors, including the angle of attack of the wheel on soil α , internal friction angle of the lunar soil ϕ , cohesion c, bulk density γ and fracture length l_0 , as shown in (32).

The angle of attack of the wheel on soil α and the fracture length l_0 can be calculated as

$$\alpha = \arccos\left(1 - \frac{2z}{D}\right) \tag{33}$$

$$l_0 = z \tan^2 \left(\frac{\pi}{4} - \frac{\phi}{2}\right) \tag{34}$$

 K_c and K_{γ} are the function factors of the Terzaghi coefficients N_q, N_c, N_{γ} , defined as follows

$$N_{q} = \frac{\exp\left[\left(\frac{3\pi}{2} - \phi\right) \tan \phi\right]}{2\cos^{2}\left(\frac{\pi}{4} + \frac{\phi}{2}\right)}$$

$$N_{c} = \cot \phi (N_{q} - 1)$$

$$N_{\gamma} = \frac{2(N_{q} + 1) \tan \phi}{1 + 0.4 \sin(4\phi)}$$
(35)

$$K_c = (N_c - \tan \phi) \cos^2 \phi$$

$$K_\gamma = \left(\frac{2N_\gamma}{\tan \phi} + 1\right) \cos^2 \phi$$
(36)

• Rolling Resistance: as the wheel of the rover rolls over the lunar surface, a force called rolling resistance is generated that opposes the motion. Lunar soil provides more resistance than a concrete floor and the rolling resistance of a vehicle has a significant impact on its motion and on its energy consumption.

This resistance is a function of rolling friction coefficient C_{rr} and load per wheel W_{wheel} and can be calculated as

$$R_r = C_{rr} \cdot W_{wheel} \tag{37}$$

where $C_{rr} = 0.05$

• Gravitational Resistance: when the vehicle moves on an inclined terrain, a component of the gravitational force opposes the vehicle's motion, generating a resistance equal to

$$R_s = W_{wheel} \cdot \sin(\theta_{slope}) \tag{38}$$

where θ_{slope} is the angle of the slope [rad].

The traction performance can be derived now, with the thrust being determined by integrating the horizontal component of the shear stress over the length of the contact zone

$$H = rb \int_{\theta_t}^{\theta_f} \tau(\theta) \cos \theta \, d\theta + (r - \delta_t) b \int_{-\theta_t}^{\theta_t} \frac{\tau(\theta)}{\cos^2 \theta} \, d\theta + rb \int_{\theta_r}^{-\theta_t} \left[\tau(\theta) \cos \theta - \sigma(\theta) \sin \theta \right] d\theta$$
 (39)

After calculating the total resistance ΣR , the net traction force, or Drawbar Pull (DP), can be estimated as the difference between the thrust, H, and the sum of the resistances

$$DP = H - \Sigma R \tag{40}$$

Considering the shear stress and the multiplication of the driving force by the corresponding arm, the torque can be obtained

$$T = r^2 b \int_{\theta_t}^{\theta_f} \tau(\theta) d\theta + (r - \delta_t)^2 b \int_{-\theta_t}^{\theta_t} \left\{ \frac{\tau(\theta) + \sigma_t \tan \theta}{\cos^2 \theta} \right\} d\theta + r^2 b \int_{\theta_r}^{-\theta_t} \tau(\theta) d\theta \qquad (41)$$

5.2 Terramechanics Simulations

For the purpose of a reliable terramechanical analysis, a preliminary selection of parameters is conducted, focusing on the characteristics of the lunar soil (Table 17).

Table 17: Soil parameters.

Soil parameter	Symbol	Value	Unit
Soil density	ρ	1680	kg/m^3
Soil weight density	γ	2721.6	N/m^3
Soil deformation exponent	n	1	-
Cohesive modulus	k_c	1370	N/m^2
Frictional modulus	k_{ϕ}	820000	N/m^3
Soil cohesion	$^{\mathrm{c}}$	170	N/m^2
Internal friction angle	ϕ	35	\deg
Shear deformation modulus	k	0.02	m
Terrain reboundness	λ	0.1	-
Wheel-soil parameter #1	a_0	0.8	-
Wheel-soil parameter $\#2$	a_1	0.15	-

To fully understand the expected terramechanical behaviour resulting from the interaction between the wheel and the lunar soil, an initial iteration is carried out to define how resistance and sinkage vary with wheel geometry, considering different diameter D and width b ranges. By selecting values of D and b that are suitable for the application considered, it is possible to show the dependence of the resistances and the sinkage on these two parameters considering the following approximate formulations [28].

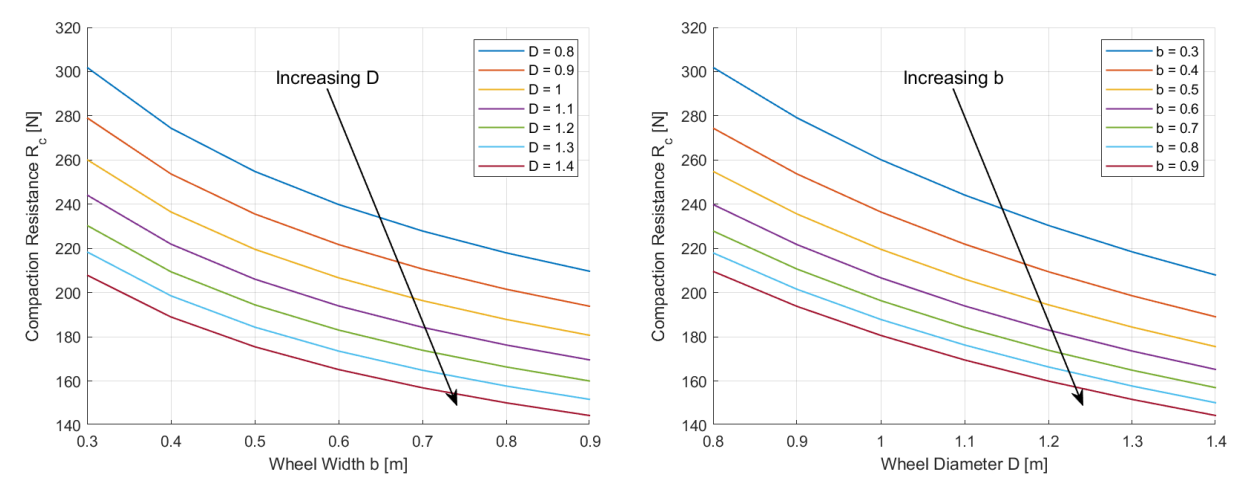
$$z = \left(\frac{3}{3 - n} \frac{W_{wheel}}{(k_c + bk_\phi)\sqrt{D}}\right)^{\frac{2}{2n+1}}$$

$$\tag{42}$$

$$R_c = \frac{1}{n+1} \left(\frac{3}{3-n} \frac{W_{wheel}}{\sqrt{D}} \right)^{\frac{2(n+1)}{2n+1}} \left(\frac{1}{k_c + bk_\phi} \right)^{\frac{1}{2n+1}}$$
(43)

$$R_b = \frac{b\sin(\alpha + \phi)}{2\sin(\alpha)\cos(\phi)} (2zcK_c + \gamma z^2K_\gamma) + \frac{l_0^3\gamma}{3} \left(\frac{\pi}{2} - \phi\right) + cl_0^2 \left[1 + \tan\left(\frac{\pi}{4} + \frac{\phi}{2}\right)\right]$$
(44)

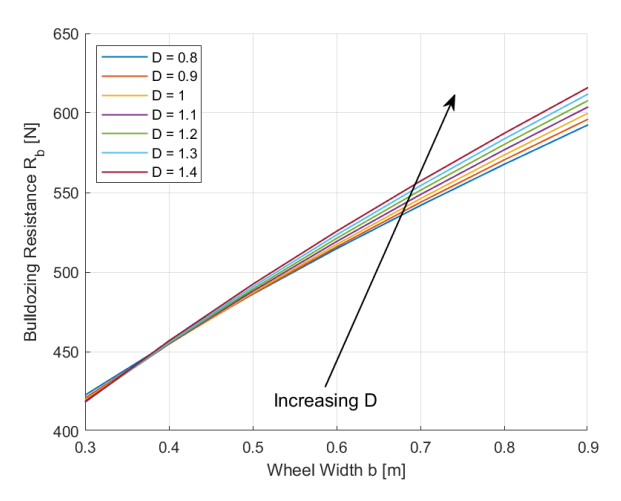
where α , l_0 , K_c and K_{γ} are calculated respectively as (33), (34), (36).

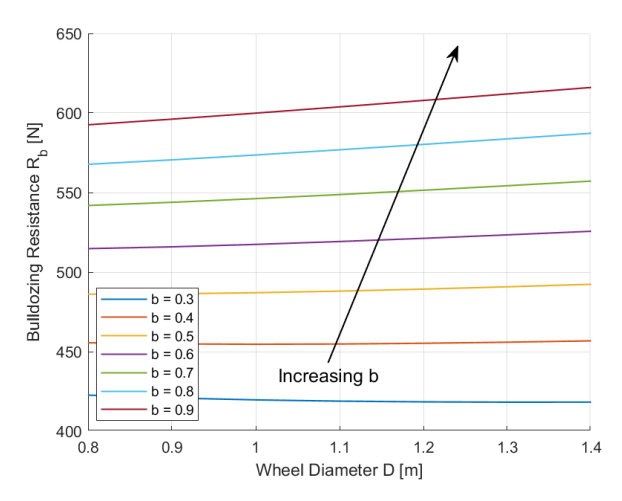


(a) R_c as a function of width b for different values of diameter D.

(b) R_c as a function of diameter D for different values of width b.

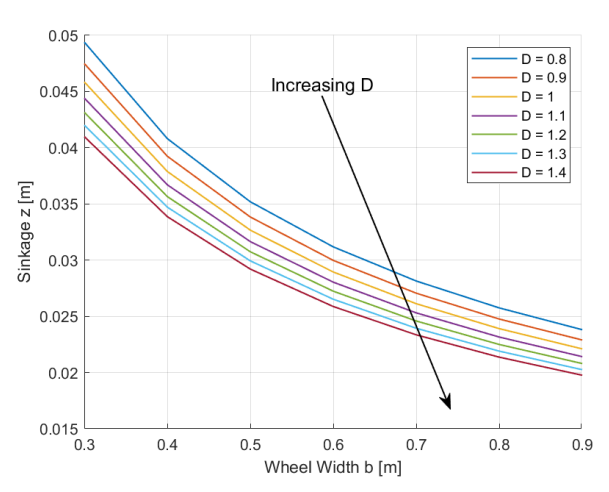
Figure 21: Compaction Resistance as a function of wheel width b and wheel diameter D.

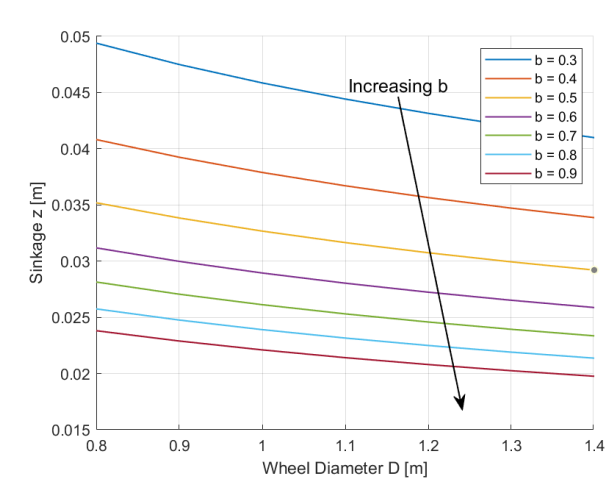




- (a) R_b as a function of width b for different values of diameter D.
- (b) R_b as a function of diameter D for different values of width b.

Figure 22: Bulldozing Resistance as a function of wheel width b and wheel diameter D.





- (a) z as a function of width b for different values of diameter D.
- (b) z as a function of diameter D for different values of width b.

Figure 23: Sinkage as a function of wheel width b and wheel diameter D.

Considering the wheel's parameters, it can be noticed that compaction resistance decreases with the increase of the wheel width and diameter (Figure 21). The influence of the wheel's width on the compaction resistance is slightly greater than the diameter, as shown in Figure 21b.

Moving to bulldozing resistance, this force tends to increase as the wheel diameter increases (Figure 22a). For higher values of wheel width the bulldozing increases, as the wheel displaces a greater volume of soil. This resistance is also affected by fracture length which depends on wheel sinkage.

The influence of wheel width on the sinkage is more significant than that of diameter. The sinkage can be reduced by increasing the width and diameter of the flexible wheel (Figure 23).

This therefore highlights the importance of optimizing wheel dimensions for the terrain considered.

5.2.1 Wheel geometry optimization

To define the dimensions of the pressurized rover's wheels, a multi-objective optimization analysis is conducted based on the terramechanical model presented above. Specifically, the design variables considered were the diameter D and width b of the wheel, geometric parameters that directly influence resistance and traction capacity on lunar soil. The optimization is performed with the purpose of simultaneously minimizing the compaction resistance, the bulldozing resistance and the sinkage.

The general single-objective optimization can be formulated as

$$\min_{\mathbf{x}} f(\mathbf{x}) \quad \text{with } \mathbf{x} \in \Omega \tag{45}$$

where f is the objective function and Ω is the feasible design domain.

In real-world application problems, multiple objectives are generally considered, where a Multi-Objective Optimization (MOO) is applied [29]. The multi-objective optimization is defined as

$$\min_{\mathbf{x}} F(\mathbf{x}) = \{ f_1(\mathbf{x}), f_2(\mathbf{x}), ..., f_m(\mathbf{x}) \}$$

$$\tag{46}$$

where f_i are the objective functions to be minimized.

The set of all solutions is called the Pareto front, where each point represents a compromise between the objectives considered.

Multi-objective optimization approach The MOO procedure is formulated through an iterative script implemented on MATLAB considering the two design variables:

$$\mathbf{x} = \{D, b\} \tag{47}$$

and the three objective functions

$$f_1(\mathbf{x}) = z(D, b), \quad f_2(\mathbf{x}) = R_c(D, b), \quad f_3(\mathbf{x}) = R_b(D, b)$$
 (48)

The optimization problem can be formulated as

$$\min_{\{D,b\}} \{ z(D,b), \ R_c(D,b), \ R_b(D,b) \}$$
(49)

taking into account the following constraints

$$\begin{cases} D_{\min} \le D \le D_{\max} \\ b_{\min} \le b \le b_{\max} \\ z(b, D) \ge 0 \end{cases}$$
 (50)

By applying Eq. (42), Eq. (43), Eq. (44) of the terramechanical model, the objective becomes:

- minimizing z to prevent excessive penetration into the soil and subsequent increase in rolling resistance;
- minimizing R_c to reduce energy losses during movement;
- minimizing R_b to avoid excessive energy demand and the forward movement more difficult.

The optimization, implemented using the MATLAB genetic algorithm *gamultiobj*, is structured into three main sections:

- 1. Definition of the function multiobjectiveThreeObj, which takes the design variables D and b as input and returns a vector containing the three functions to be minimized, calculated from terramechanical formulations.
- 2. Definition of parameters relating to the rover, such as total mass, number of wheels and normal load per wheel; definition of parameters of the lunar soil, such as cohesion, weight density, exponent of sinkage, cohesive modulus, frictional modulus and internal friction angle (Table 17).
- 3. Definition of the design constraints for D and b into realistic ranges for a pressurized rover:

$$0.3 \le b \le 0.9, \quad 0.8 \le D \le 1.4$$
 (51)

This process returns a set of Pareto-optimal solutions, each characterized by an optimal combination of wheel diameter and width.

The results show that an increase in diameter tends to reduce sinkage by distributing the load more evenly, but can increase bulldozing resistance. An increase in width reduces the specific pressure on the ground, thereby reducing the compaction resistance, but the bulldozing resistance tends to increase with the area of disturbance. The solutions obtained do not converge to a single optimal point, but provide a framework of compromises. The three-dimensional plot in Figure 24 illustrates the entire Pareto front, enabling a global evaluation of the interaction between the three objectives. The selection of the final geometry requires a compromise between the various alternatives, evaluating the priorities of the mission: if the project is oriented towards safety in mobility, solutions with reduced sinkage but higher resistance are preferred; if the priority becomes energy efficiency, the focus shifts on solutions that lower resistances while tolerating an increase in sinkage.

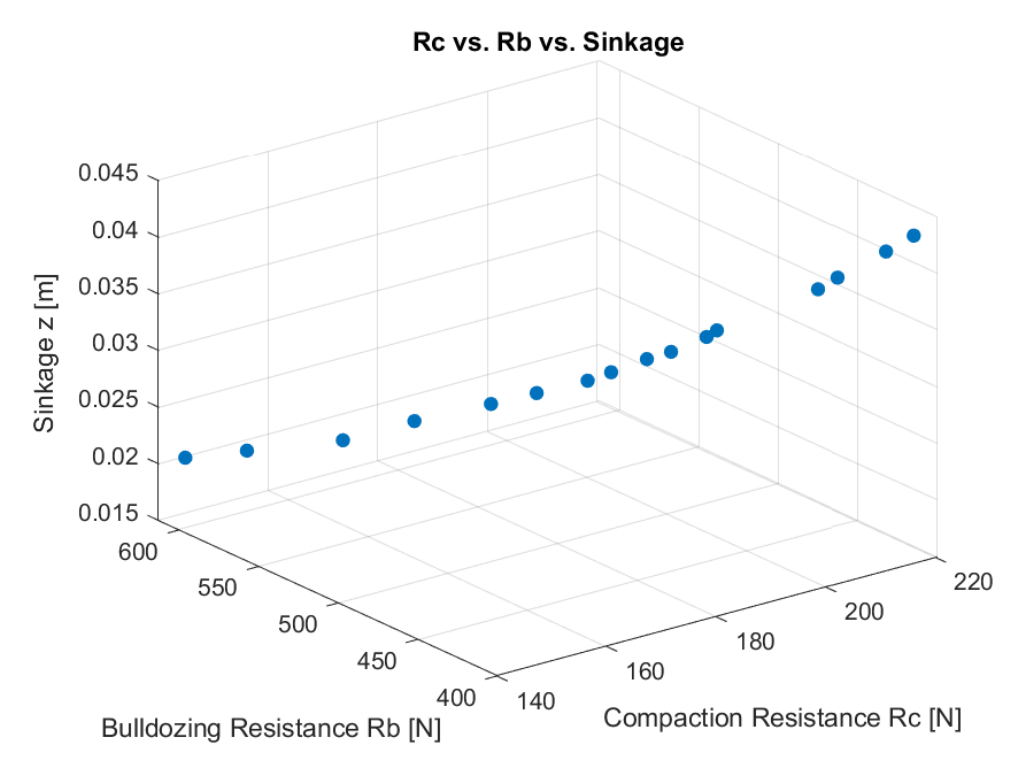


Figure 24: Representation of the Pareto-optimal solutions.

Following trade-offs, the configuration that provides the most effective compromise between mobility and energy efficiency is D = 1.2 m and b = 0.4 m.

This solution offers a good balance, allowing for low sinkage to reduce the risk of immobilization while ensuring adequate traction and preventing resistance from exceeding acceptable levels.

5.3 Terramechanics results

Once the optimization phase is complete, the terramechanical model is implemented using the selected wheel diameter and width values. In particular, using the above analytical formulations, the model enables the calculation of:

- the distribution of normal and tangential stresses on the contact area (Eq. (22), Eq. (29));
- the thrust generated (Eq. (39));
- the total resistance during motion;
- the drawbar pull, obtained from the difference between the available thrust and the total resistance (Eq. (40));
- the torque required at the wheel hub to ensure motion (Eq. (41)).

Below, Figure 25 shows the evolution of H, R and DP as a function of the wheel pressure P_w .

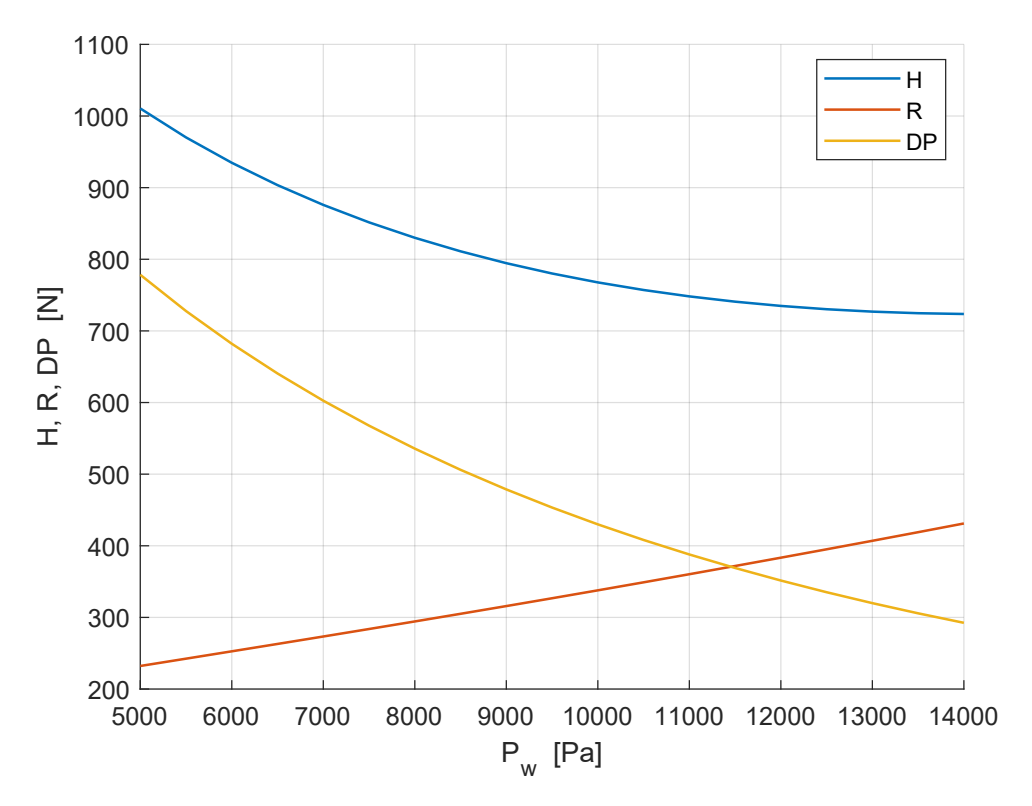


Figure 25: Evolution of thrust, resistance and drawbar pull as a function of wheel pressure P_w .

It can be observed that as Pw increases, the thrust H tends to decrease, while the resistance tends to increase. The DP, given by the difference between thrust and resistance, tends to decrease until it assumes a negative value. This trend is consistent with terramechanical theory, confirming that high Pw values reduce traction effectiveness, as the resistance exceeds the available thrust. Moreover, discussing in detail the single contributions:

(a) Decreasing tractive effort $H(P_w)$. For constant wheel load W, an increase in effective wheel pressure P_w reduces the contact length l_t and the vertical deflection δ . This reduces the shear displacement $j(\theta)$:

$$j(\theta) = r \left[(\theta_f - \theta) - (1 - s) \left(\sin \theta_f - \sin \theta \right) \right].$$

Consequently, the exponential term in

$$\tau(\theta) = (c + \sigma(\theta) \tan \phi) \left(1 - e^{-j(\theta)/K}\right),$$

approaches a lower asymptote for higher P_w . The local shear stress $\tau(\theta)$ therefore decreases, and the integral tractive effort H tends to diminish. This behavior matches the analytical and experimental curves reported by Wong [26] for reduced contact length and low slip ratios.

- (b) Increasing total resistance $R(P_w)$. The total resistance R in this formulation includes: the compaction component, the slope resistance, the internal rolling loss, and the bulldozing term. Among these, the compaction term scales approximately with the normal stress at the front of the wheel, which is a function of P_w . Although the sinkage δ decreases with P_w , the normal stress distribution at the leading edge can rise faster, causing R to increase. This trend is also compatible with the Wong [26] bulldozing-resistance models.
- (c) Drawbar pull $DP(P_w)$. The drawbar pull DP = H R decreases with increasing P_w , remaining positive, since H = R (DP = 0) occurs only when the available tractive capacity equals the total resistances:

$$H = R_{\text{comp}} + R_{\text{slope}} + R_{\text{roll}} + R_{\text{bulldozing}}.$$

For the current parameters ($\phi = 37.2^{\circ}$, c = 170 Pa, s = 0.05, rf = 0.05 and flat slope) the soil is relatively strong and the slip ratio low, leading to sustained positive drawbar pull. An intersection H = R appears when either:

- the slope angle increases (raising R_{slope});
- the rolling-resistance factor rf is higher;
- the shear deformation modulus K increases (reducing τ);
- the cohesion c or friction angle ϕ decrease (weaker soil).

All these variations are physically motivated within Bekker's [19] and Wong's [26] framework.

Assuming a reasonable pressure value of $P_w = 11000 \ Pa$ as the design point, the values obtained (Table 18) show that the rover is capable of developing sufficient positive traction to ensure mobility on lunar terrain.

Table 18: Terramechanical results for $P_w = 11000 \ Pa$.

Quantity	Value
Thrust H	748.1819 N
Resistance R	360.3093 N
Drawbar Pull DP	387.8726 N
Torque T	419.8280 Nm

5.4 Wheels design

Simultaneously with the development of the terramechanical model, a multi-criteria analysis based on the Analytic Hierarchy Process (AHP) method [30] is conducted to perform

a preliminary comparative evaluation between the different wheel configurations. This approach allows for the quantification of judgments on the relative importance of multiple design criteria, translating them into normalized weights that express the contribution of each attribute to the overall decision. The following four candidate wheel configurations are considered for the analysis:

- Flexible metal wheel
- Airless tire wheel
- Ellipse spring wheel
- Metallic mesh wheel

Each configuration was evaluated against five key performance attributes, derived from the literature on planetary mobility systems and consistent with the design objectives of the pressurized rover:

- load capacity, as the ability to support expected static and dynamic loads with adequate safety margins;
- traction, as the ability to transmit torque and maintain adherence in variable regolith conditions;
- adaptability to terrain, as the ability to conform to uneven and deformable surfaces, ensuring stable contact and overcoming obstacles;
- resistance to lunar dust, which includes resistance to abrasion and performance degradation caused by lunar regolith;
- durability, regarding the expected duration and resistance to mechanical fatigue under conditions of thermal and mechanical stress.

Through pair comparisons between the criteria, the AHP method allows relative importance weights to be assigned based on their functional contribution to the rover's mobility. Table 19 shows the Prioritization Matrix of the AHP for the wheel: each entry in the row expresses its importance in relation to the relative column. The diagonal is always equal to 1 (equal importance with itself), while the respective row-column elements outside the diagonal are reciprocal $(a_{ij} = 1/a_{ji})$.

Table 19: Wheel's AHP Prioritization Matrix.

Prioritization Matrix	Load capacity	Traction	Adaptability to terrain	Resistance to lunar dust	Durability
Load Capacity	1	0.5	3	5	2
Traction	2	1	3	5	3
Adaptability to terrain	0.333	0.333	1	4	0.5

Resistance to lunar dust	0.2	0.2	0.25	1	0.333
Durability	0.5	0.333	2	3	1
Normalized weights	0.271	0.392	0.125	0.053	0.159

The prioritization matrix reveals the following hierarchy of criteria, expressed in terms of normalized weights:

- 1. Traction ~ 0.392 :
- 2. Load capacity ~ 0.271 ;
- 3. Durability \sim 0.159;
- 4. Adaptability to terrain ~ 0.125 ;
- 5. Resistance to lunar dust~0.053.

This distribution reflects the functional logic of a pressurized vehicle designed to operate on the lunar surface, where mobility is the key enabling factor for the entire mission.

Traction is a primary priority, as for a heavy vehicle such as the one in question, loss of grip and consequent immobilization on slopes or low-cohesion regolith represents the dominant risk.

Load capacity is the second most influential criterion, as a wheel capable of adequately supporting static and dynamic loads prevents excessive sinking and reduces the loads transmitted to the suspension.

Next is durability, which is particularly important over longer distances, where thermal cycles and impacts have a negative effect on the wheel's fatigue resistance and wear, leading to a gradual deterioration in traction performance and reliability.

Adaptability to the terrain has also a relevant position, but part of this requirement is mitigated by the vehicle's suspension architecture.

Finally, resistance to lunar dust completes the robustness of the design, but this is fairly manageable through the choice of suitable materials and coatings, so its relative weight is lower than the failure modes of loss of mobility.

The weights obtained are subsequently used to assess each wheel concept, resulting in a quantitative hierarchy of alternatives. As an example, Table 20 shows the comparison matrix between wheel configurations based on the criterion of load capacity. Further matrices relating to the comparison between wheels are shown in Appendix B.

Table 20: Example: wheel's load capacity.

Load capacity	Flexible Metal Wheel	Airless tire Wheel	Ellipse Spring Wheel	Metallic Mesh Wheel
Flexible Metal Wheel	1	0.2	3	6

Airless tire Wheel	5	1	5	7
Ellipse Spring Wheel	0.333	0.2	1	2
Metallic Mesh Wheel	0.167	0.143	0.5	1

The first-level analysis identifies the Flexible Metal Wheel and the Airless Tire Wheel as the most promising solutions, showing the best balance between structural and operational performances (Figure 26). These two configurations are therefore selected for a second comparative analysis, aimed at considering dimensional, mechanical, and environmental constraints in more detail.

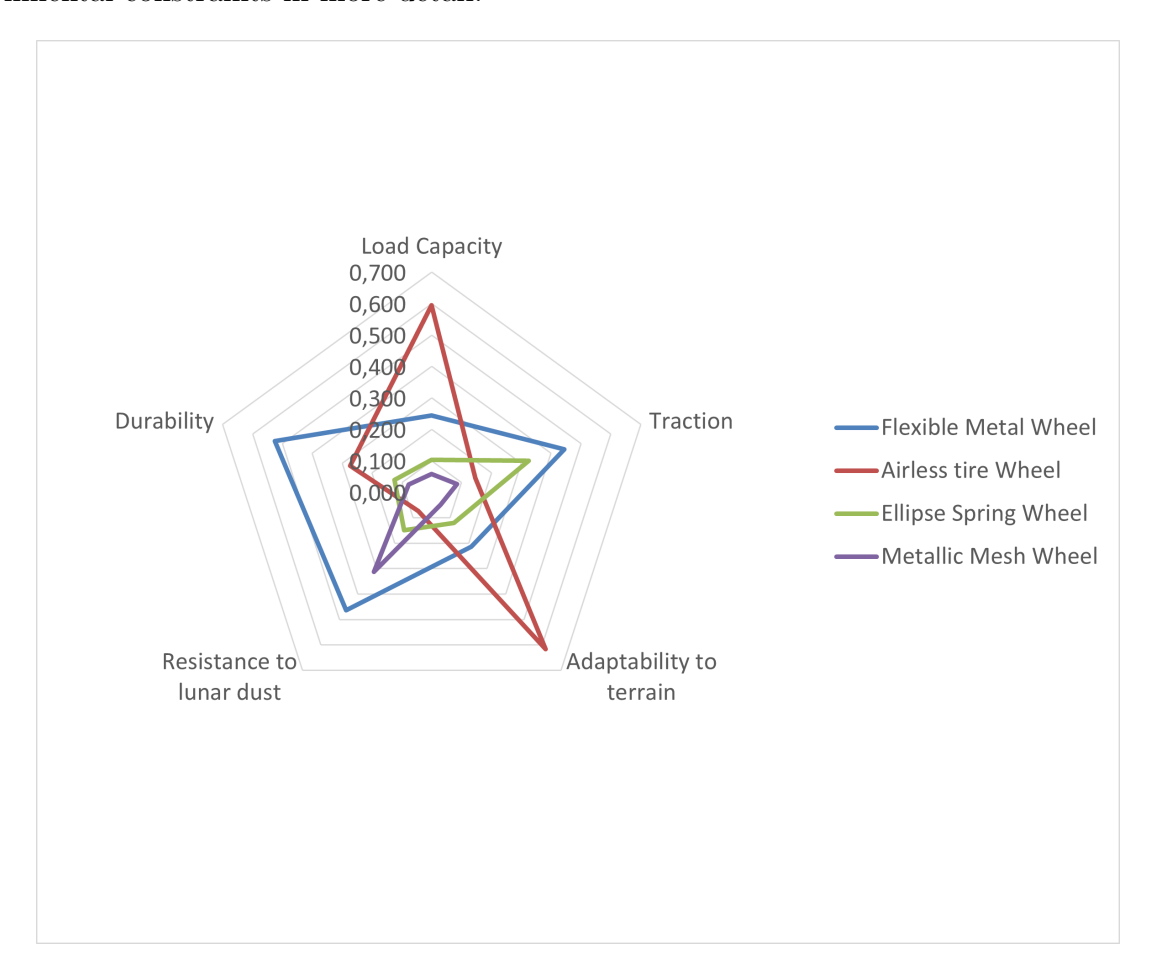


Figure 26: AHP results for wheels.

5.4.1 Wheel type

Flexible Metal Wheel The flexible metal wheel is one of the most established solutions for mobility applications in extraterrestrial environments. It was originally devel-

oped by the NASA Glenn Research Center to equip the Lunar Roving Vehicle (LRV) used during the Apollo missions (1971–1972). The design featured a structure made of a high-strength steel woven mesh, capable of adapting to the terrain and withstanding the roughness of the lunar surface. For the LRV, however, the wheel was designed for significantly lower loads than those of the rover covered in this study: each wheel of the Apollo vehicle supported approximately 300 N, compared to the more than 1800 N expected for each wheel of the pressurized rover.

As a result, the traditional mesh wheel design required significant structural improvement to ensure the necessary mechanical strength while maintaining flexibility and terrain adaptation performance. To meet the requirement for higher loads, a flexible metal wheel version is being considered. This design features a spring steel sheets double carcasses joined by connecting rings, while the tread is made of a series of "X-shape" strings. The working principle involves the elastic deformation of the spring steel sheets upon contact with the ground, causing an increase in the contact surface and reducing contact pressure. This effect consequently guarantees a reduction in sinkage and an increase in dynamic comfort. The deformation of the wheel also provides a slight suspension effect, resulting in the damping of small shocks and vibrations. This wheel offers numerous advantages from both functional and environmental perspectives:

- no risk of bursting or loss of pressure for the tire;
- thermal resistance to lunar operating temperatures;
- tolerance to radiation and abrasive dust;
- reduced sinkage;
- high traction.

Despite its advantages, this configuration also exhibits some limitations, including:

- higher construction complexity;
- fatigue phenomena for extended load cycles;
- higher weight due to the use of the mentioned materials.

Airless Tire Wheel The second option considered is the airless wheel made of composite elastomeric material, derived from terrestrial concepts such as Michelin's UPTIS [31]. The spokes, made of high-strength resin embedded fiberglass, are directly connected to the rim and have high resilience, excellent load-carrying capacity, and vibration-damping properties, which improve driving comfort. The main advantages offered by the airless wheel include:

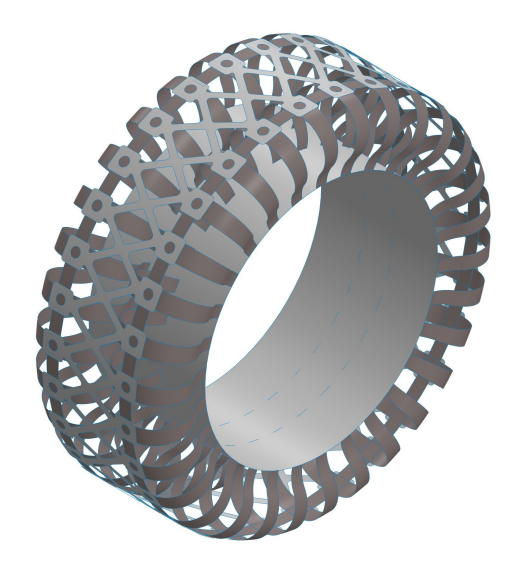
- no risk of bursting or loss of pressure for the tire;
- puncture or sharp objects impact resistance;
- adaptability to terrain;
- built-in shock absorption.

However, this type of wheel has significant disadvantages that must be taken into consideration, such as:

• degradation of materials at lunar temperature range;

- risk of infiltration of abrasive and electrostatic dust;
- low traction in soft granular soil.

The two wheel concepts investigated for the preliminary design are illustrated in Figure 27, highlighting the structural differences between the flexible metal wheel and the airless tire configuration.





- (a) Flexible Metal Wheel (simplified model)
- (b) Airless Tire Wheel

Figure 27: Types of wheels considered for the preliminary design.

5.4.2 Comparative analysis

The comparative analysis is conducted considering several factors arising from operating conditions on the lunar surface, such as traction capacity, structural reliability, and environmental compatibility. Each criterion was assigned a score from 1 to 5 (1 = poor performance, 5 = excellent performance). The results of the assessment are shown in Table 21.

Table 21: Wheel comparative analysis.

Trade-off criterion	Flexible Metal Wheel	Airless Tire Wheel
Sinkage	4	3
Traction DP	5	2
Dynamic comfort	4	4
Thermal resistance	5	2
Dust and radiation resistance	4	2

Total	30	22
Manufacturing complexity	2	3
Application heritage	3	2
Mass	3	4

The comparison shows that the flexible metal wheel is the most suitable solution for the considered mission. This type of tire shows greater adaptability to the terrain, allowing for low sinkage and greater traction, improving the rover's energy efficiency. Although the airless wheel is an interesting emerging technology, it is limited by lunar environmental conditions, which exceed the thermal and mechanical capabilities of currently available elastomeric materials.

5.5 Suspension Architecture

The suspension subsystem plays a fundamental role in ensuring the stability and dynamic comfort of the rover when traveling over uneven surfaces. Its architecture directly influences the distribution of loads on the wheels, the ability to maintain contact with the ground, and the reduction of vibrations transmitted to the structure and occupants, thus contributing to both operational safety and component durability. Several suspension types suitable for planetary vehicles are analyzed:

- passive suspension represents the most consolidated solution, offering high reliability and reduced construction complexity;
- semi-active suspension introduces the possibility of real-time variation of damping and stiffness;
- active suspension (full active) employs independent electromechanical or hydraulic actuators capable of generating control forces, allowing the vehicle's attitude to be maintained and compensating for uneven terrain;
- hybrid suspension presents a passive platform integrated with active elements, which provide support in specific critical conditions.

Even for the trade-off analysis aimed at selecting the type of suspension, a series of performance attributes are identified for the evaluation of the different configurations. In particular, the following comparison criteria are considered:

- adaptability, which refers to the suspension's capability to conform to the terrain profile while keeping stable contact between the wheels and the surface. This concept is primarily geometric-static and quantifies how adequately the suspension system will compensate for height differences without loss of grip or extreme variations in the chassis balance;
- maneuverability, intended as the kinematic attribute that measures the effectiveness of the system in managing roll, pitch, and lateral and longitudinal load;

- ride comfort, classified as part of the dynamic attributes, indicates the suspension's ability to decouple the vehicle habitat and occupants from vibrations and shocks, assessing how much the system mitigates the accelerations transmitted from the wheel-ground contact point to the structure;
- design complexity, defined as the degree of mechanical and electronic complexity of the system;
- cost/mass/power demand, which summarizes the impact of suspension on resources, such as development and integration costs, mass increase, and power demand during operations.

As performed for the wheels, the AHP method [30] is also applied to the suspensions to visualize the most suitable configurations.

Table 22: Suspension's AHP Prioritization Matrix.

Prioritization Matrix	Adaptability	Maneuverability	Ride comfort	Design complexity	Cost/mass/power demand
Adaptability	1	2	1	3	2
Maneuverability	0.5	1	2	2	2
Ride comfort	1	0.5	1	3	1
Design complexity	0.333	0.5	0.333	1	0.333
Cost/mass/power demand	0.5	0.5	1	3	1
Normalized weights	0.300	0.246	0.201	0.082	0.171

The prioritization matrix for the suspension reveals the following hierarchy of criteria, expressed in terms of normalized weights:

- 1. Adaptability ~ 0.300 ;
- 2. Maneuverability~0.246;
- 3. Ride comfort ~ 0.201 ;
- 4. Cost/mass/power demand ~ 0.171 ;
- 5. Design complexity~0.082.

The hierarchy resulting from the prioritization matrix reflects the operational requirements of a pressurized lunar rover. By assigning greater importance to factors related to the dynamic performance of the system, the weighting hierarchy favors adaptability and maneuverability, since for a pressurized lunar rover the ability to adapt to uneven terrain and maintain maneuverability on slopes and obstacles is essential to ensure stability and safety. Ride comfort is also a determining factor, as it directly influences the well-being of the crew and the integrity of the module. Although cost/mass/power demand has a minor weight, it remains relevant to design since in modern missions these aspects are closely monitored in order to conserve resources and improve overall efficiency. The design complexity criterion, even if relevant, is the least influential, as greater complexity is accepted as long as it results in better response and reliability.

The comparison performed between the pairs of configurations (Appendix B) returns the result shown in Figure 28.

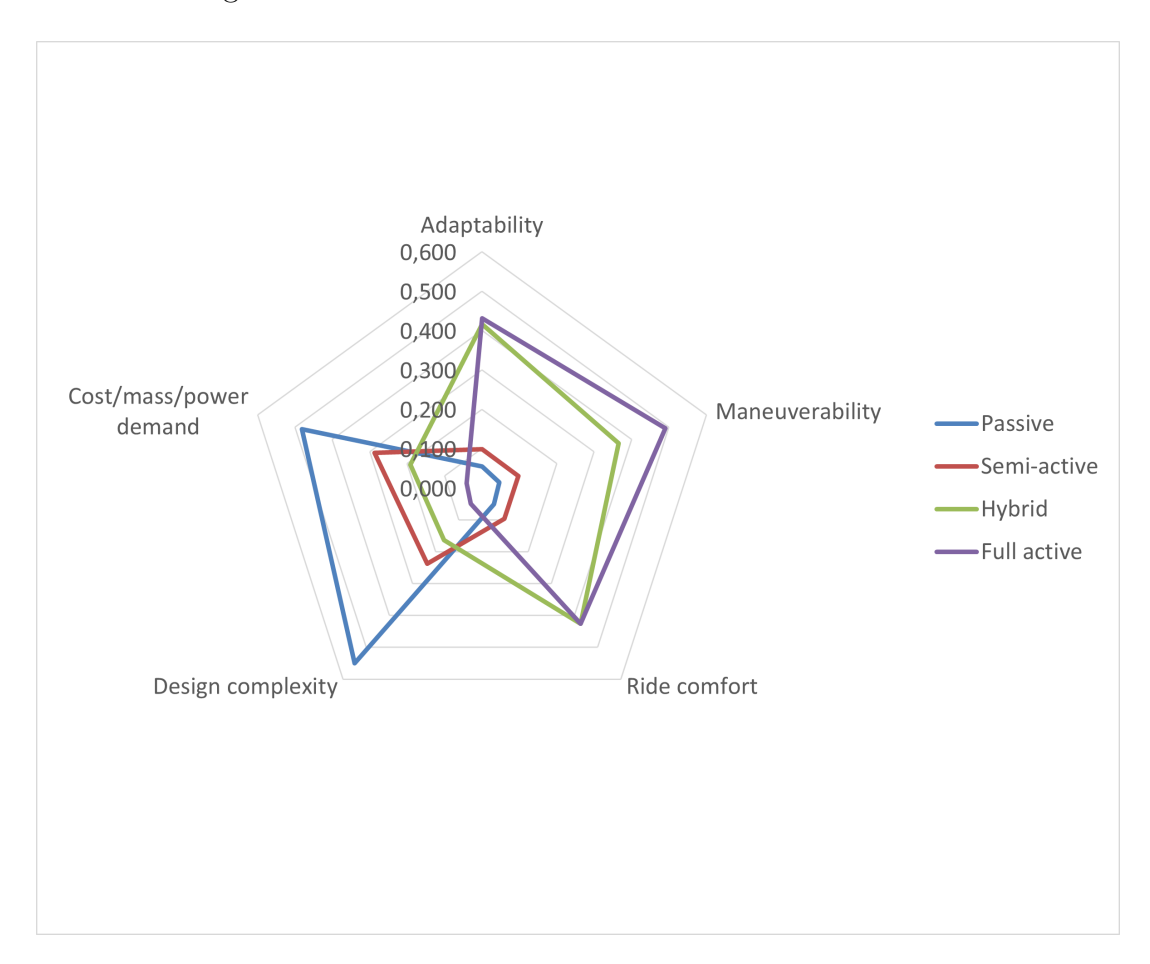


Figure 28: AHP results for suspension.

In this preliminary phase, the considered architecture is a hybrid suspension that operates passively under nominal conditions. It features an electromechanical actuator that activates under critical or necessary operating conditions, such as overcoming obstacles, leveling on slopes and aligning with the primary habitat during the docking phase. The choice derives from a compromise between simplicity and the need for punctual corrective actions, in an environment that penalizes the use of alternative technologies such as hydraulic circuits, where fluid-based systems would suffer from issues related to out-gassing, evaporation and long-term seal integrity.

5.5.1 Hybrid suspension model

For the local study of the vertical dynamics of a single suspension, a 2 DOF quarter-car model [32] is adopted for each of the six suspension units of the rover. The suspension unit consists of

- m_s : sprung mass per wheel;
- m_u : unsprung mass (wheel + axle);
- k_s : suspension stiffness;
- c_s : suspension damping;
- k_t : wheel vertical stiffness;
- c_t : wheel damping;
- F_a : actuator force;
- z_s, z_u, z_r : vertical displacements from static equilibrium of the sprung mass, unsprung mass and the terrain.

Figure 29 shows the diagram representing the hybrid suspension model adopted.

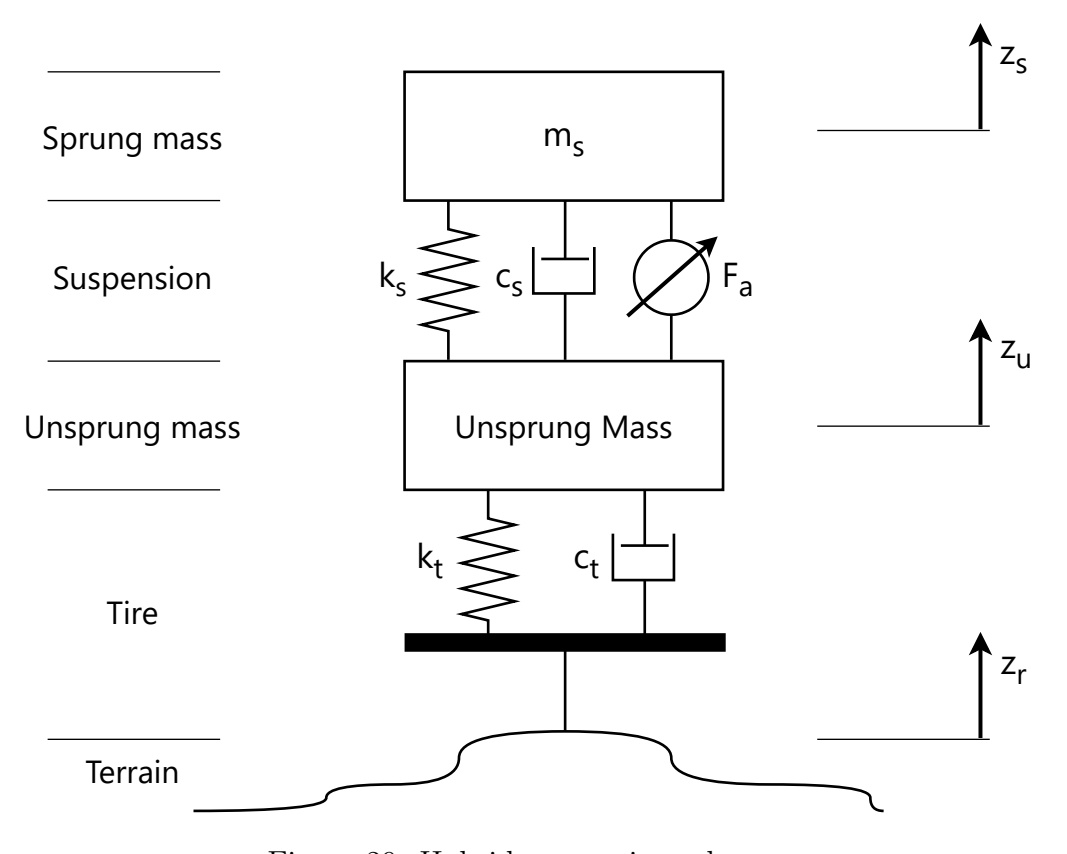


Figure 29: Hybrid suspension scheme.

The equations of motion are

$$m_s \ddot{z}_s + c_s (\dot{z}_s - \dot{z}_u) + k_s (z_s - z_u) = F_a$$
 (52)

$$m_u \ddot{z}_u - c_s (\dot{z}_s - \dot{z}_u) - k_s (z_s - z_u) + k_t (z_u - z_r) + c_t (\dot{z}_u - \dot{z}_r) = -F_a$$
 (53)

The equations of motion can be expressed using the absolute coordinates of the two masses as state variables. The state vector is defined as

$$x = \begin{bmatrix} x_1 & x_2 & x_3 & x_4 \end{bmatrix}^T = \begin{bmatrix} z_s \\ \dot{z}_s \\ z_u \\ \dot{z}_u \end{bmatrix}$$
 (54)

and considering the matrix form of the system, the space state model is obtained

$$\dot{x} = Ax + B_f F_a + B_{z_r} z_r + B_{\dot{z}_r} \dot{z}_r, \tag{55}$$

where

$$A = \begin{bmatrix} 0 & 1 & 0 & 0 \\ -\frac{k_s}{m_s} & -\frac{c_s}{m_s} & \frac{k_s}{m_s} & \frac{c_s}{m_s} \\ 0 & 0 & 0 & 1 \\ \frac{k_s}{m_u} & \frac{c_s}{m_u} & -\frac{k_s + k_t}{m_u} & -\frac{c_s + c_t}{m_u} \end{bmatrix}, \qquad B_f = \begin{bmatrix} 0 \\ \frac{1}{m_s} \\ 0 \\ -\frac{1}{m_u} \end{bmatrix}, \tag{56}$$

$$B_{z_r} = \begin{bmatrix} 0 \\ 0 \\ 0 \\ \frac{k_t}{m_u} \end{bmatrix}, \qquad B_{\dot{z}_r} = \begin{bmatrix} 0 \\ 0 \\ 0 \\ \frac{c_t}{m_u} \end{bmatrix}.$$

Matrix A collects the coefficients of the internal dynamics of the system (masses, springs, dampers); the B_f matrix contains the input coefficients relating to the active force F_a ; the matrices B_{z_r} and $B_{\dot{z}_r}$ represent, respectively, the effect of the road profile and its speed on the system, linked to the stiffness and damping of the tire.

This formulation in absolute coordinates allows the ground profile to be introduced as input $(z_r(t), \dot{z}_r(t))$ and the dynamic response of the two masses to be observed in terms of absolute displacement and velocity.

The conditions for activating the actuator are based on comparing the kinematic and dynamic variables with specific thresholds derived from dynamic analyses and simulations. Active behavior switch thresholds can be:

- $|z_u z_r| > \delta_z$: the deflection of the wheel relative to the terrain profile exceeds a certain margin;
- $|\phi_{roll}| > \phi_{roll,lim}, |\theta_{pitch}| > \theta_{pitch,lim}$: the roll and pitch angles $(\phi_{roll}, \theta_{pitch})$ of the main body exceed the maximum inclination and a leveling maneuver must be implemented;

- $z_{obs} > z_{obs,lim}$: the obstacle height estimated by the sensors exceeds the obstacle threshold limit;
- $||e_{dock}|| > e_{dock,lim}$: the alignment error in position and orientation for docking exceeds the tolerance.

In case one or more of these conditions are encountered, the control system switches from passive to active mode, commanding the actuator to generate the corrective force F_a . This condition can be expressed in a compact form as

$$u = \begin{cases} 0 & if \ C_{act}(z_u - z_r, \phi, \theta, z_{obs}, e_{dock}) \le 0, \\ F_a & if \ C_{act}(z_u - z_r, \phi, \theta, z_{obs}, e_{dock}) > 0 \end{cases}$$

$$(57)$$

where u is the active force control signal, while C_{act} is a Boolean condition which determine the operating mode of the system.

Case study: overcoming an obstacle z_{obs} To verify the adaptive capacity of the hybrid suspension system, a numerical simulation is conducted to reproduce the behavior of a single suspension unit when overcoming an isolated obstacle. This study aims to provide a qualitative understanding of the transition between passive and active modes, rather than quantitative validation, examining the related effects on the displacement of the suspended mass.

The analysis initially involves defining the essential parameters for the simulation: sprung mass for each wheel $(m_s = 0.85 * (M_{tot}/n_{wheels} kg))$ and unsprung mass for each wheel $(m_u = 0.15 * (M_{tot}/n_{wheels} kg))$, suspension stiffness $(k_s = 120 \ kN/m)$, suspension damping $(c_s = 4 \ kNs/m)$, wheel vertical stiffness $(k_t = 250 \ kN/m)$ and wheel damping $(c_t = 0.7 \ kNs/m)$ for each suspension unity). The values, consistent with those reported in the literature, are selected to optimize the response and represent a starting point for the next iterations of optimization.

The excitation profile of the terrain is modeled as an obstacle with height $z_{obs} = 0.3 m$ and length $L_{obs} = 1.0 m$, overcome at a constant speed of v = 20 km/h; these values are used to determine the time interval $[t_0, t_1]$ corresponding to wheel-obstacle interaction.

During this time interval, a skyhook-type active control of the suspension system is enabled, generating the control force F_a .

The equations of motion describing dynamic behavior are expressed in the form of the space state model (Eq.55). Outside the activation window, the actuator remains deactivated, restoring only the passive response.

The simulation involves evaluating two modes:

- passive mode, without any action by the actuator;
- hybrid mode, with control activation only in the specified window.

For preliminary considerations, the simulation aims to return the vertical displacement of the suspended mass $z_s(t)$ for both modes as a function of time Figure 30.

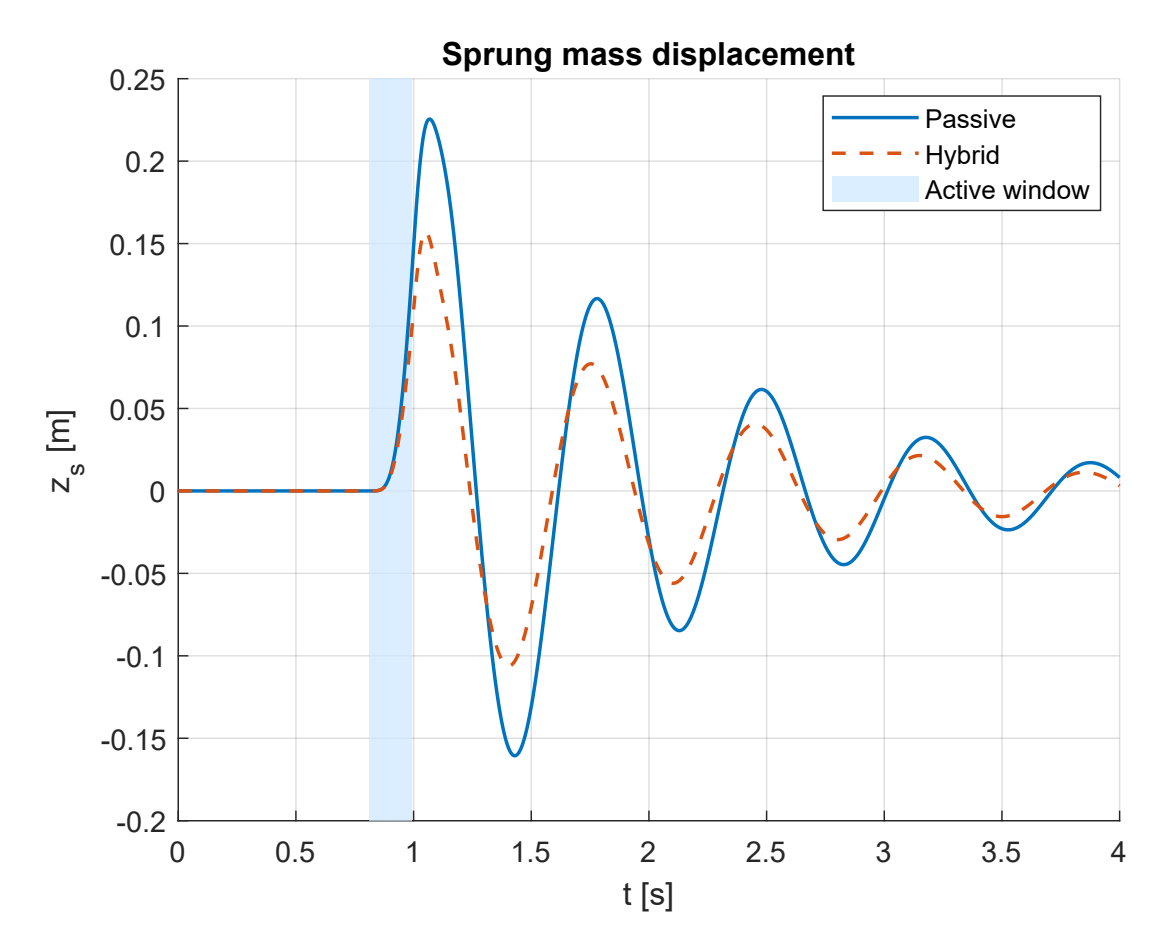


Figure 30: Vertical displacement of the sprung mass.

The comparison of the two modes shows that in the initial section (before the obstacle) the two configurations coincide perfectly, as expected: the actuator is deactivated and the system behaves like a purely passive suspension.

When overcoming the bump, the passive suspension shows a greater displacement peak, which corresponds to the direct response of the suspended mass to the excitation of the terrain. On the other hand, the hybrid suspension attenuates this peak through its control action, which opposes a force proportional to the speed of the suspended mass. The effect is a reduction in the maximum amplitude of displacement and a faster dissipation of subsequent oscillations.

Finally, after the end of the active window, the two trends tend to coincide again, confirming that the hybrid system returns to passive behavior, ensuring stability and dynamic continuity.

6 Discussion

This section analyses the results through a perspective which shows how analytical findings affect lunar mission design. The evaluation includes a summary of system strengths and weaknesses based on current methods which suggests directions for future work to improve system maturity.

6.1 Terramechanical methodological approach

The terramechanical approach based on Bekker's model proved to be an effective starting point for predicting wheel performance on lunar soil. This analytical formulation clearly shows how each physical parameter (such as wheel size or soil stiffness) directly affects traction and sinkage.

The model provides a demonstration of how wheels deform by using a combined static and dynamic system which connects wheel forces to wheel design and weight. This allowed for a clear estimation of several outputs, such as thrust, drawbar pull, and resistance.

The results should be interpreted as a first approximation that outline useful trends and operational design ranges. Future research can expand this model with finite element analyses or numerical simulations on regolith simulants to verify stress distributions and local deformation.

The main advantage of the chosen framework is its flexibility. The same structure can be applied to more complex simulations, for example by incorporating dynamic models or control algorithms for traction management. In this sense, the method does not just provide numerical results but offers a structured basis for subsequent design phases.

6.2 Wheel geometry optimization logic

The genetic multi-objective optimization connected the physical model to the design process, allowing analytical equations to become an actual tool for engineering choices. By considering the wheel diameter (D) and width (b) as design variables, the effect of geometry on mobility and efficiency could be estimated.

Optimization results showed the Pareto front which demonstrated distinct physical compromises between different solutions. Increasing the diameter improves load distribution and reduces sinkage but it leads to bigger power needs and heavier equipment. Increasing the width reduces sinkage but it leads to higher bulldozing resistance. The final selected configuration, D=1.2 m and b=0.4 m, represents a balanced solution, giving sufficient traction with moderate torque demand and resistance losses.

These values are consistent with current lunar rover concepts such as NASA's SEV [9] and JAXA's Lunar Cruiser [10], showing that the model reflects realistic design scales. The analysis also suggests that small changes in tire pressure or slip ratio can significantly alter traction, reinforcing the idea that manned rovers may benefit from controlled wheel actuation or adaptive drive systems.

6.3 Evaluation of wheel concepts

The AHP evaluation complemented the analytical study by introducing a structured way to compare different wheel concepts against mission requirements. While the terramechanical model quantified physical performance, the AHP provided a multi-criteria assessment considering aspects such as manufacturability, durability, and environmental resistance.

Among the concepts analyzed, the flexible metal wheel was evaluated the highest. Its design achieves both structural strength and flexibility, ensuring strong traction performance and environment resistance.

Airless tire wheels demonstrate potential for Earth applications, yet face multiple challenges in the lunar environment. Both the wide temperature range and abrasive dust create a harsh environment, which results in polymers degradation. Metal mesh or spring designs, on the other hand, remain mechanically reliable and easier to maintain, but still unsuitable for use in heavier rovers.

Adopting a metallic flexible wheel also simplifies mechanical integration with the suspension system, since it avoids materials sensitive to vacuum or radiation. The remaining concern is fatigue under repeated cycles, which will need to be verified through detailed FEM simulations.

The integration of terramechanics and AHP highlights that combining quantitative analysis with qualitative rational analysis can lead to more balanced decisions in the early design stages.

6.4 Suspension trade-offs

Suspension design is a key driver for both safety and comfort. For a crewed pressurized rover, the system must isolate the cabin from shocks while remaining reliable and energy efficient. Passive architectures, such as rocker-bogie or double A-arm systems, are mechanically simple and highly reliable but transmit more vibration. Fully active suspensions, while effective, are heavy and power-hungry.

The hybrid suspension proposed in this work unites the benefits from both the previous configurations. A passive spring–damper stage absorbs vibrations, while limited electromechanical actuation is used to control vehicle attitude, slope alignment, and docking height. This solution offers a suitable trade-off between adaptability and simplicity.

Compared to magnetorheological or hydraulic systems, which would struggle with dust and outgassing issues, electromechanical actuators are better candidate for the lunar environment. The hybrid system can also be operated safely in fail-safe mode: even in case of an actuator failure, the passive components can maintain the essential mobility of the vehicle.

From an operational perspective, this architecture supports adjustable ground clearance, slope compensation, and improved comfort for the crew. Future work should evaluate

actuator power consumption and response times to ensure compatibility with available electrical power.

6.5 Integrated system implications

The locomotion subsystem must work as part of a larger integrated vehicle. The selected cylindrical pressurized module, 7.1 m long and 3.07 m in diameter, offers high structural efficiency and a low center of gravity. Combined with the optimized wheel geometry and hybrid suspension, it ensures static stability even on 20° slopes.

The external dimensions (4.17 m height, 4.10 m width) remain compatible with standard launch fairings, such as those of Falcon Heavy or Starship. This confirms that mobility components can be integrated without exceeding launch or deployment constraints.

6.6 Comparison with state-of-art designs

When compared with modern rover projects, the proposed configuration aligns closely with current technological trends. Both NASA's SEV[9] and JAXA's Lunar Cruiser[10] use electric drivetrains, metallic compliant wheels, and modular structures. The hybrid suspension approach adds a realistic next step in mobility system evolution, combining proven reliability with selective adaptability.

The optimization and trade-off process introduced in this work provides a more formal and analytical basis than typically found in conceptual design studies. It connects system-level decisions (mass, geometry, range) with the associated engineering models, improving traceability between mission requirements and design parameters.

6.7 Limitations of the analysis

The work also has limitations that define directions for future refinement. The terrame-chanical model assumes homogeneous, isotropic soil, while the real lunar regolith varies with depth and location. The friction angle and cohesion can change significantly, affecting traction. A sensitivity analysis would be valuable to quantify the uncertainty range.

Dynamic effects such as slip or wheel acceleration were not included. These could be studied through time domain simulations or discrete element models. Structural aspects such as load and vibration were treated parametrically and require FEM-based verification.

Finally, the AHP prioritization relies partly on expert judgment. As experimental data become available, these weights could be refined through data-driven calibration. Recognizing these limits is important to guide the transition from analytical feasibility to engineering maturity.

6.8 Implications for lunar exploration architecture

The methodology developed in this work provides a replicable process that connects mission requirements, physical models, and system integration.

The analytical and optimization techniques adopted are compatible with model-based engineering approaches and can be implemented within tools such as *Capella* or *Valispace*. This would allow requirements, analyses, and design iterations to remain connected in a single environment, promoting collaborative design consistent with concurrent engineering logic.

6.9 Synthesis

This work demonstrates that a structured, physics-based design approach can effectively guide the early development of a lunar rover locomotion system. The main outcomes can be summarized as follows:

- analytical terramechanics provides a practical foundation for predicting performance on lunar soil;
- multi-objective optimization identifies wheel geometries that balance sinkage and resistances;
- the flexible metal wheel offers the best compromise between strength, compliance, and thermal resistance;
- a hybrid suspension improves comfort and adaptability without adding extreme complexity;
- the overall configuration is compatible with launch vehicle constraints.

The collected data confirm the technical feasibility of the proposed locomotion concept and define a clear roadmap for its future development. The next steps can involve structural FEM analyses of the flexible wheel, dynamic testing of the hybrid suspension, and experimental validation on lunar soil simulants. These activities represent the connection between the preliminary design to a fully qualified mobility system for the lunar pressurized rover.

7 Conclusion and future work

This thesis presented the preliminary design and analysis of the locomotion system for a lunar pressurized rover intended for future human exploration missions. The work combined analytical modeling, optimization, and system-level reasoning to define a coherent and realistic design capable of operating in the harsh lunar environment.

The initial analysis of soil conditions and existing rover architectures led to the definition of mobility requirements, which were then translated into design parameters relating to wheel geometry, performances, and suspension configuration.

The analytical model based on Bekker's terramechanics proved to be effective in describing wheel-soil interaction and providing a quantitative basis for the initial design stages, which can be further refined with numerical simulations on soil simulants.

The multi-objective optimization of the wheel geometry enabled to identify a balance between efficiency, traction, and structural constraints. The chosen configuration (1.2 m in diameter and 0.4 m wide) is consistent with the most advanced projects (such as NASA SEV and Lunar Cruiser) and represents a balanced compromise between performance and integrability.

Through the Analytic Hierarchy Process (AHP), different wheel concepts were compared based on key performance parameters such as traction, load capacity, durability, adaptability and environmental resilience. The flexible metallic wheel emerged as the most promising option: it offers structural flexibility and abrasion resistance with high thermal durability. In contrast, polymeric alternatives appeared less suitable due to their sensitivity to extreme temperature variations and dust.

For the suspension system, a hybrid solution was proposed, combining passive elements with electromechanical actuation. The passive part guarantees reliability, while the active component provides leveling, slope adaptation and alignment functions during docking. This architecture avoids the limitations typical of hydraulic or magnetorheological systems, offering an effective compromise between robustness, performance and controllability.

However, several aspects require further investigation. The current terramechanical model assumes homogeneous and isotropic soil, while lunar regolith varies depending on location and depth. Dynamic effects, such as wheel acceleration or slip and sinkage coupling, should be included to better describe real driving conditions.

A detailed finite-element analysis (FEM) of the wheel structure can represent a key next step. This approach would allow the evaluation of local stress distributions, cyclic deformations, and stress concentration points, particularly at the joints and reinforcements of the flexible metal structure. Integrating FEM results with the terramechanical model would also allow the definition of more accurate stiffness and compliance parameters, which would be useful for dynamic simulations.

Beyond the current design, future developments should explore alternative wheel concepts, such as deformable or honeycomb structures inspired by airless tire concept. These

configurations, if made with materials suitable for the lunar environment, could offer better damping capabilities and adaptability to lunar terrain.

Additionally, the terramechanical model can be extended to analyze non-linear operating cases, such as steering maneuvers, which introduces significant lateral and tangential stresses that can alter the load distribution and soil compaction beneath the wheel. Modeling these conditions would enable a more complete understanding of vehicle behavior during turning, traversing, or obstacle overcoming and would support more precise control strategies for stability enhancement.

To conclude, the research validates that achieving reliable and effective locomotion for a multi-ton lunar pressurized rover can be achieved through a balance of analytical modeling, optimization, and integrated system design. The methodology created can be utilized for reference to support conceptual and preliminary design of the system .

A Abbreviations

AHP Analytic Hierarchy Process

BDTM Bekker's Derived Terramechanics Model

BMS Battery Management System

CDH Command and Data Handling

COMMS Communication System

DP Drawbar Pull

ECLSS Environmental Control and Life Support Systems

ECSS European Cooperation for Space Standardization

EMU Extravehicular Mobility Unit

EPS Electrical Power System

GNC Guidance, Navigation and Control

GTO Geostationary Transfer Orbit

IMU Inertial Measurement Unit

ISRU In Situ Resource Utilization

LEO Low Earth Orbit

LER Lunar Electric Rover

LPR Lunar Pressurized Rover

LRV Lunar Roving Vehicle

LTO Lunar Transfer Orbit

MOO Multi-Objective Optimization

NHV Net Habitable Volume

PDU Power Distribution Unit

SEV Space Exploration Vehicle

SoW Statement of Work

TCS Thermal Control System

B AHP tables

B.0.1 Wheels

Table 23: Traction.

Traction	Flexible Metal Wheel	Airless tire Wheel	Ellipse Spring Wheel	Metallic Mesh Wheel
Flexible Metal Wheel	1	4	2	3
Airless tire Wheel	0.25	1	0.333	3
Ellipse Spring Wheel	0.5	3	1	5
Metallic Mesh Wheel	0.333	0.333	0.2	1

Table 24: Adaptability to terrain.

Adaptability to terrain	Flexible Metal Wheel	Airless tire Wheel	Ellipse Spring Wheel	Metallic Mesh Wheel
Flexible Metal Wheel	1	0.2	3	5
Airless tire Wheel	5	1	6	8
Ellipse Spring Wheel	0.333	0.167	1	4
Metallic Mesh Wheel	0.2	0.125	0.25	1

Table 25: Resistance to lunar dust.

Resistance to lunar dust	Flexible Metal Wheel	Airless tire Wheel	Ellipse Spring Wheel	Metallic Mesh Wheel
Flexible Metal Wheel	1	5	3	2
Airless tire Wheel	0.2	1	0.5	0.167
Ellipse Spring Wheel	0.333	2	1	0.5
Metallic Mesh Wheel	0.5	6	2	1

 ${\bf Table\ 26:}\ {\it Durability}.$

Durability	Flexible Metal Wheel	Airless tire Wheel	Ellipse Spring Wheel	Metallic Mesh Wheel
Flexible Metal Wheel	1	3	4	5
Airless tire Wheel	0.333	1	3	4
Ellipse Spring Wheel	0.25	0.333	1	2
Metallic Mesh Wheel	0.2	0.25	0.5	1

Table 27: AHP Summary for Lunar Rover Wheel Concepts

Summary	Loa Capa		Trac	tion	Adapta to ter	•	Resist to luna		Dural	oility	Final Score
	Weight	Score	Weight	Score	Weight	Score	Weight	Score	Weight	Score	
Flexible Metal Wheel	0.271	0.244	0.392	0.444	0.125	0.214	0.053	0.464	0.159	0.526	0.375
Airless Tire Wheel	0.271	0.595	0.392	0.146	0.125	0.616	0.053	0.073	0.159	0.273	0.343
Ellipse Spring Wheel	0.271	0.103	0.392	0.325	0.125	0.121	0.053	0.149	0.159	0.124	0.198
Metallic Mesh Wheel	0.271	0.058	0.392	0.085	0.125	0.049	0.053	0.314	0.159	0.077	0.084

B.0.2 Suspension

Table 28: Adaptability.

Adaptability	Passive	Semi-active	Hybrid	Full active
Passive	1	0.333	0.167	0.143
Semi-active	3	1	0.167	0.167
Hybrid	6	6	1	1
Full active	7	6	1	1

Table 29: Maneuverability.

Maneuverability	Passive	Semi-active	Hybrid	Full active
Passive	1	0.333	0.125	0.125
Semi-active	3	1	0.167	0.2
Hybrid	8	6	1	0.5
Full active	8	5	2	1

Table 30: Ride comfort.

Ride comfort	Passive	Semi-active	Hybrid	Full active
Passive	1	0.333	0.143	0.143
Semi-active	3	1	0.167	0.167
Hybrid	7	6	1	1
Full active	7	6	1	1

Table 31: Design complexity.

Design complexity	Passive	Semi-active	Hybrid	Full active
Passive	1	3	4	8
Semi-active	0.333	1	2	5
Hybrid	0.25	0.5	1	5
Full active	0.125	0.2	0.2	1

 ${\it Table 32: } {\it Cost/mass/power demand.}$

Cost/mass/power demand	Passive	Semi-active	Hybrid	Full active
Passive	1	2	3	9
Semi-active	0.5	1	2	7
Hybrid	0.333	0.5	1	7
Full active	0.111	0.143	0.143	1

References

- [1] N. Patel, R. Slade, and J. Clemmet. The exomars rover locomotion subsystem. 47(4): 227–242. ISSN 0022-4898. doi: 10.1016/j.jterra.2010.02.004.
- [2] NASA. Artemis: Returning humans to the moon, 2024. URL https://www.nasa.gov/humans-in-space/artemis/. Accessed: 2025-07-18.
- [3] J. J. Zakrajsek, D. B. McKissock, J. M. Woytach, J. F. Zakrajsek, F. B. Oswald, K. J. McEntire, G. M. Hill, P. Abel, D. J. Eichenberg, and T. W. Goodnight. Exploration rover concepts and development challenges. In *Proceedings of the First AIAA Space Exploration Conference*, pages 12–19. NASA, 2005.
- [4] G. H. Heiken, D. T. Vaniman, and B. M. French. *Lunar Sourcebook*. Cambridge University Press, 1991.
- [5] M. Malenkov. Self-propelled automatic chassis of lunokhod-1: History of creation in episodes. 11(1):60–86. ISSN 2095-0241. doi: 10.1007/s11465-016-0370-5.
- [6] J. Heldmann and J. O. Elliott. Inspire in situ solar system polar ice roving explorer. Technical report, NASA. URL https://science.nasa.gov/wp-content/uploads/2023/10/inspire-lunar-polar-volatiles-rover.pdf.
- [7] J. T. Keane, S. M. Tikoo, and J. Elliott. Endurance, lunar south pole-aitken basin traverse and sample return rover. Technical report, NASA. URL https://science.nasa.gov/wp-content/uploads/2023/11/endurance-spa-traverse-and-sample-return.pdf.
- [8] T. Lund. Lunar Roving Vehicle and Exploration of the Moon, pages 303–324. Springer International Publishing. ISBN 9783030020712. doi: 10.1007/978-3-030-02071-2_10.
- [9] NASA. Space exploration vehicle concept. Technical report. URL https://www.nasa.gov/wp-content/uploads/2015/08/464826main_sev_factsheet_508.pdf?emrc=0855ca.
- [10] T. M. Corporation. Toyota's lunar cruiser: from earth to the moon and back. URL https://www.toyota-europe.com/news/2023/lunar-cruiser.
- [11] E. Rollins, J. Luntz, A. Foessel, B. Shamah, and W. Whittaker. Nomad: a demonstration of the transforming chassis. In *Proceedings. 1998 IEEE International Conference on Robotics and Automation (Cat. No.98CH36146)*, volume 1 of *ROBOT-98*, pages 611–617. IEEE. doi: 10.1109/robot.1998.677040.
- [12] J. O. Elliott. Concept for a radioisotope powered dual mode lunar rover. In AIP Conference Proceedings, volume 813, pages 898–905. AIP. doi: 10.1063/1.2169272.
- [13] B. GRIFFIN, D. THRASHER, and B. WALLACE. A pressurized rover for early lunar exploration. In *Space Programs and Technologies Conference*. American Institute of Aeronautics and Astronautics. doi: 10.2514/6.1992-1488.
- [14] K. Creel, J. Frampton, D. Honaker, K. McClure, and M. Zeinali. Pressurized lunar rover. Technical report, Virginia Polytechnic Institute and State University, NASA.

- [15] M. Bhardwaj, V. Bulsara, D. Kokan, S. Shariff, E. Svarverud, and R. Wirz. Design of a pressurized lunar rover. Technical Report NASA-CR-192033, National Aeronautics and Space Administration (NASA), 1992. URL https://ntrs.nasa.gov/api/citations/ 19930008827/downloads/19930008827.pdf.
- [16] R. Arno. Human Spaceflight: Mission Analysis and Design. New York: McGraw-Hill and Co. ISBN 007236811X.
- [17] J. C. Mankins. Modular architecture options for lunar exploration and development. 51st International Astronautical Congress.
- [18] D. Akin and M. Bowden. Morphlab: Modular roving planetary habitat, laboratory, and base. In Space 2004 Conference and Exhibit. American Institute of Aeronautics and Astronautics. doi: 10.2514/6.2004-6034.
- [19] M. Bekker. Theory of Land Locomotion: The Mechanics of Vehicle Mobility. University of Michigan Press. ISBN 9780472913572. doi: 10.3998/mpub.9690401.
- [20] P. Berkelman, J. Easudes, M. C. Martin, E. Rollins, and J. Silberman. *Design of a Day/Night Lunar Rover*. doi: 10.21236/ada310807.
- [21] I. A. Crawford. Lunar resources: A review. 39(2):137–167. ISSN 1477-0296. doi: 10.1177/ 0309133314567585.
- [22] European Cooperation for Space Standardization. ECSS-E-ST-10-06C, 2009. Available online. URL: https://ecss.nl/wp-content/uploads/standards/ecss-e/ECSS-E-ST-10-06C6March2009.pdf (Accessed on 13 Dec 2024).
- [23] Design for ionizing radiation protection. Technical Report NASA-STD-3001 Technical Brief, NASA Office of the Chief Health and Medical Officer (OCHMO), 2023. URL https://www.nasa.gov/wp-content/uploads/2023/12/ochmo-tb-020-radiation-protection.pdf.
- [24] F. Ruess, J. Schaenzlin, and H. Benaroya. Structural design of a lunar habitat. 19(3): 133–157. ISSN 1943-5525. doi: 10.1061/(asce)0893-1321(2006)19:3(133).
- [25] N. Aeronautics and S. Administration. Human integration design handbook (hidh). techreport NASA/SP-2010-3407, NASA. URL https://www.nasa.gov/wp-content/uploads/2015/03/human_integration_design_handbook_revision_1.pdf.
- [26] J. Y. Wong. Theory of Ground Vehicles. John Wiley and Sons, Inc., 2001.
- [27] J. Mitchell, W. N. Houston, W. D. Carrier, and N. Costes. Apollo soil mechanics experiment s-200. Technical Report NASA-CR-134306, National Aeronautics and Space Administration (NASA), 1974. URL https://ntrs.nasa.gov/api/citations/19740019219/downloads/19740019219.pdf.
- [28] D. L. Akin. Terramechanics 1: Passive rolling resistance. Lecture slides, ENAE 788X Planetary Surface Robotics, University of Maryland. Available at https://spacecraft.ssl.umd.edu/academics/788XF22/788XF22L06.terramechanics1_r1x.pdf (Accessed on 06 Mar 2025).

- [29] K. Deb. *Multi-objective optimization using evolutionary algorithms*. Wiley-Interscience series in systems and optimization. Wiley, repr. edition. ISBN 047187339X.
- [30] R. Saaty. The analytic hierarchy process—what it is and how it is used. 9(3-5):161-176. ISSN 0270-0255. doi: 10.1016/0270-0255(87)90473-8.
- [31] Michelin. Michelin uptis prototype. URL https://middle-east.michelin.com/en/michelin-uptis-prototype. Accessed on 20 May 2025.
- [32] R. Rajamani. *Vehicle dynamics and control*. Mechanical Engineering Ser. Springer, second edition edition. ISBN 9781461414322.